# On buoyant convection in binary solidification

**B.S. OKHUYSEN and D.N. RIAHI**

Department of Theoretical and Applied Mechanics, 216 Talbot Laboratory, 104 South Wright Street, University of Illinois at Urbana-Champaign, Urbana, IL 61801, USA

We consider the problem of nonlinear steady buoyant convection in horizontal mushy layers during the solidification of binary alloys. We investigate both cases of zero vertical volume flux and constant pressure, referred to as impermeable and permeable conditions, respectively, at the upper mush-liquid interface. We analyze the effects of several parameters of the problem on the stationary modes of convection in the form of either hexagonal cells or non-hexagonal calls such as rolls, rectangles and squares. No assumption is made on the thickness of the mushy layer, and a number of simplifying assumptions made in previous nonlinear analyses are relaxed here in order to study a richer set of phenomena. Using both analytical and computational methods, we determine the steady solutions to the weakly nonlinear problem by using a perturbation technique for both constant and variable permeability, referred to as passive and reactive mushy layer cases, respectively. Both nonlinear basic state and reactive mushy zone of the present problem favor hexagon-pattern convection. The results of the analyses and computations indicate, in particular, that depending on the range of values of the parameters, bifurcation to non-hexagonal convection can be either supercritical or subcritical, while bifurcation to hexagon pattern convection, corresponding to the smallest value of the Rayleigh number, is subcritical. For reactive mushy layers, subcritical down-hexagons with down-flow at the cell centers and up-flow at the cell boundaries, which have been observed in related experiments (Tait, Jahrling & Jaupart 1992) , and supercritical non-hexagons were predicted in particular range of values of the parameters.

## 1. Introduction

The present study considers the problem of finite-amplitude steady convection in horizontal mushy layers during the directional solidification of binary alloys. The present investigation is based on combined analytical and computational methods to derive qualitative information about buoyant convection in mushy layers. Although a weakly nonlinear analysis of buoyant convection in binary-alloy solidification is undertaken in the present study, many of the simplifying assumptions made in previous weakly nonlinear analyses (Amberg & Homsy 1993; Anderson & Worster 1995; Chung & Chen 2000) are relaxed in order to study a richer set of phenomena.

The simplified mushy-layer model was introduced first by Amberg & Homsy (1993). The model was based on a neareutectic approximation and in the limit of large far-field temperature. It was used to examine the dynamics of the mushy layer in the regime of small deviation from the classical system of convection in a horizontal porous layer of constant permeability. Such single-layer model for an actual two-layer model for an alloy directional solidification system (Worster 1992) focused on the mushy-layer mode of convective flow, which is one of the two modes of buoyant convection discovered by Worster

(1992) in the two-layer system. To construct such a single-layer model for the mushy zone, Amberg & Homsy (1993) needed to make a number of simplifying assumptions including those stated above and the ones that the thickness of the mushy layer is small and such layer is isolated from the overlying liquid layer. In addition, the authors assumed that the amplitude of convection is of the same order as the thickness of the mushy layer. The finite-amplitude steady convection studied in Amberg & Homsy (1993) was limited to two-dimensional rolls and hexagons only. The authors found that two-dimensional rolls were supercritical for sufficiently small values of the deviation of the permeability from a constant value and subcritical if such deviation was not too small, and steady hexagons were found to be transcritical.

Anderson & Worster (1995) extended the analytical studies of Amberg & Homsy (1993) to the limit of large Stefan number $\mathscr{S}$, which represents the latent heat release due to solidification, and the case $\epsilon^2 \ll \delta \ll 1$. The authors applied a double-series expansion in powers of and for the rescaled variables and the Rayleigh number R. They focused on the steady modes of convection and calculated, in particular, the finite amplitude steady solutions in the form of two-dimensional rolls and hexagons. Chung & Chen (2000) modified the boundary conditions of the Amberg & Homsy (1993)'s model, replacing the condition of no vertical volume flux at the top boundary with a condition of constant pressure. This alteration results in mushy layer that is more coupled to the melt above. The found better agreement with the results of two-layer linear analysis (Worster 1992)

To date, the phenomena observed by Tait *et al.* (1992) remains unaccounted for in theory. The hexagonal planform they observed suggests that an understanding of the physical mechanisms of chimney formation should be accessible via a weakly nonlinear analysis. However, the nonlinear analyses undertaken thus far have not produced satisfactory results consistent with the observation. This lack of consistency may be due to the assumption of thin mushy layer. While this assumption renders the problem analytically tractable, the inconsistency with experimental results suggests that some extension is needed. Here, although a weakly nonlinear analysis of buoyant convection in mushy layers is undertaken, many of the simplifying assumptions made in previous nonlinear analyses are relaxed in order to study a richer set of phenomena. The price of this extended range is that the expressions of the nonlinear analysis are no longer analytical.

The approach taken here is to use weakly nonlinear analysis (Busse 1967) to study the effect of finite amplitude perturbations. A series of boundary value problems is obtained. While the mathematical systems governing these problems do not yield analytical solutions, solutions may be obtained by straightforward one-dimensional numerical techniques for integration and boundary value problems. The technique incorporates both analytical and computational methods to derive qualitative information about buoyant convection in mushy layers. Such a hybrid methodology has not yet been employed to study convection in a mushy layer.

In the present investigation we carry out analyses and computations for two cases. For the first case, we consider the condition where the mushy layer is assumed to be isolated from the overlying liquid layer in the solidification system, so that the condition of no vertical volume flux of flow at the top boundary, like that considered in Amberg & Homsy (1993) and Anderson & Worster (1995), is employed. For the second case of the present investigation, we follow Chung & Chen (2000) and replace such upper boundary condition for the vertical volume flux by a condition of constant pressure. As these authors demonstrated, the condition of constant pressure implies the condition of zero vertical rate of change of the vertical velocity. This alteration in the upper boundary condition results in mushy layer that is more coupled to the melt above. Chung & Chen (2000) , who studied the Amberg & Homsy (1993)'s model subjected to such alteration

in the upper boundary condition, found better agreement with the results of two-layer linear analyses (Worster 1992).

One of the main goals to study buoyant convection during the solidification of binary alloys has often been to understand convection in the mushy layer and in chimneys leading to a class of defects called freckles, which is of particular concern in binary alloys. Freckles are roughly cylindrical chimney regions in the solidified materials that are depleted in solute and often have anisotropically oriented grains. They form along the direction of solidification and cause a disruption of compositional homogeneity. Freckles are commonly found in cast binary alloys such as nickel-aluminum, aluminum-copper and lead-tin, as well as steel. Copley, Giamei, Johnson & Hornbecker (1970) investigated the origin of freckles by studying the freezing of aqueous ammonium chloride solutions. Previous studies of freckles were performed on quenched alloy samples, but Copley *et al.* (1970) noted that ammonium chloride-water solution was phenomenological similar to solidifying alloys. By using an aqueous analog of a metal system, they were able to view fluid flow during solidification. They found that in such a system, convective jets flowing upward through the mushy layer cause freckles. Thus, clearly understanding the convection in mushy layers and the mechanisms of chimney development is an important problem. In the present investigation we study convection and different types of patterns that could be predicted in mushy layers. Ultimately, the goal will be to understand chimney formation in the mushy layers and then to leverage our understanding to inhibit chimney formation. By reducing chimneys, we can reduce or eliminate freckles and thus improve important manufacturing processes involving metal alloys. Here we take the first step toward understanding chimneys by studying convection in the mushy layer and elucidating the preferred flow patterns in a more physical model of the solidifying alloy through an analysis of weakly nonlinear solutions. Finally, it should be noted that although the discussion has been framed in terms of metallurgy, an understanding of these processes has many applications in other fields, including crystal growth, geophysics and geology.

The following two sections 2 and 3 deal with the mathematical formation of the problem and the analyses. The results of the steady convection for permeable and impermeable mush-liquid interface are presented and discussed respectively, in sections 4 and 5, which are followed by the conclusion and some remarks in section 6.

## 2. Mathematical formulation

### 2.1. *The model*

A binary alloy undergoing solidification at a constant speed $V$ is considered. This system can be realized by the so-called gradient freeze technique in materials manufacturing, for which the liquid melt is drawn at constant speed through a fixed temperature gradient. Solidification takes place in a container, or ampoule. Morphological instability at the solidification front, induced by constitutional undercooling, causes a distinct mushy layer to form between the completely solidified material and the liquid melt. As the alloy solidifies with a given composition, it releases buoyant residual fluid within the mushy layer. A schematic description of this physical system is shown in figure 1.

In contrast to pure substances, changes in phase in multi-component materials do not occur at a single temperature. A binary phase diagram characterizes the equilibrium phase behavior of a binary alloy. A representative binary phase diagram is shown in figure 2. The point E is the eutectic point. When a cooling melt with eutectic composition CE passes through the eutectic temperature TE, the liquid phase is transformed into the

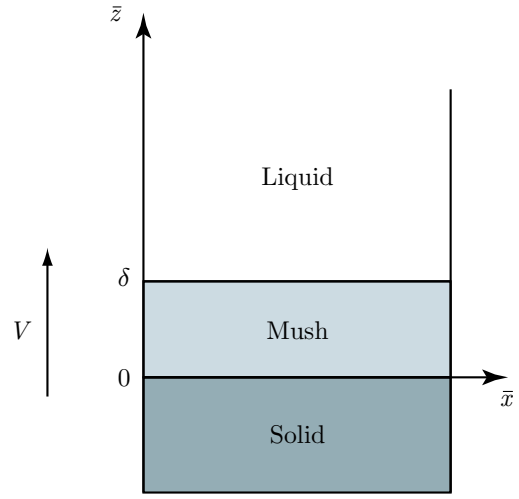


FIGURE 1. Schematic diagram representing the physical system under consideration. The mush of constant thickness grows upward into the liquid melt at a rate $V$.

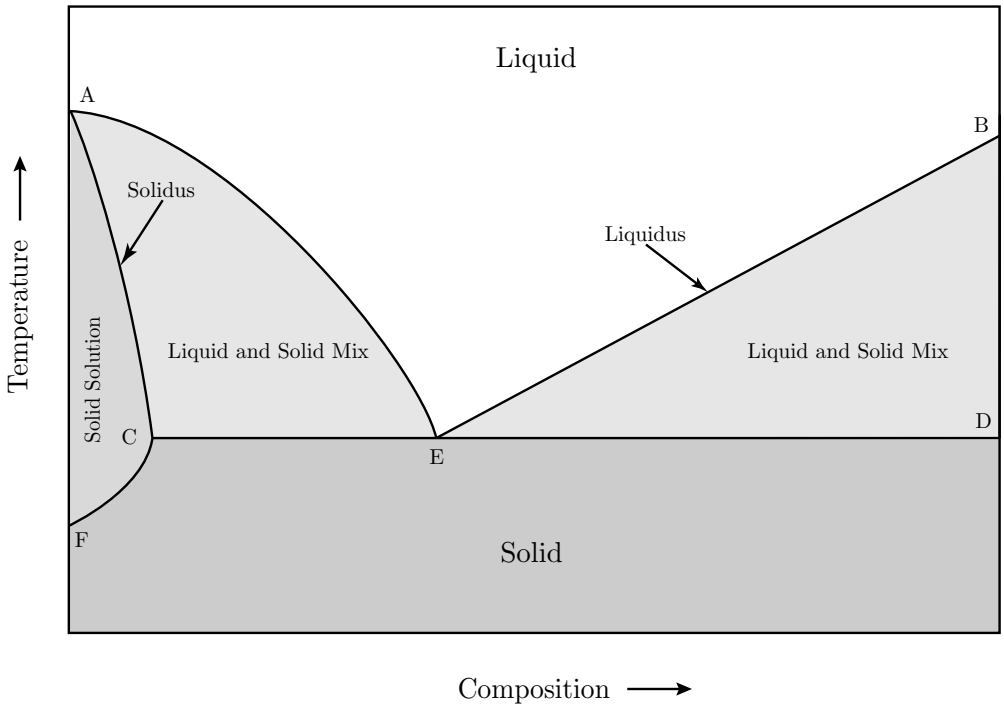


FIGURE 2. Representative binary phase diagram.

two distinct phases. The region ACF represents material of a single phase, in which atoms of one component are incorporated into the lattice of the other to form a solid solution.

It is often the case in aqueous solutions and binary alloys that solidification of a melt results in a solid phase of a pure component. We assume that the concentration of the melt $C_0$ is greater that the eutectic concentration $C_E$. When local thermodynamic equilibrium in the mush is assumed, a point in the region EBD of the phase diagram

in figure 2 describes the state of the mushy layer. The concentration of the liquid is then related to the temperature in the mush by the liquidus. It is well known that the liquidus is nearly linear in a large number of aqueous and binary alloy systems and so it is assumed that

$$T = T_L(C) = T_E + \Gamma(C - C_E), \tag{2.1}$$

where $T$ is the temperature, $C$ is the composition and $\Gamma$ is the constant slope of the liquidus. The density of the fluid l is expressed in terms of its temperature and composition as

$$\rho_l = \rho_0[1 - \alpha^*(T - T_E) + \beta^*(C - C_E)], \tag{2.2}$$

where $\alpha^*$ and $\beta^*$ are expansion coefficients for heat and solute, respectively, and $\rho_0$ is a reference value for the density. Using (2.1) in (2.2), the equation of state may then be written

$$\rho_\mathrm{l} = \rho_0[1 - (\alpha^*\Gamma - \beta^*)(C - C_\mathrm{E})], \tag{2.3}$$

Solidification shrinkage is neglected, so $\rho_\mathrm{s} = \rho_\mathrm{l}$, where $\rho_\mathrm{s}$ is the density of the solid.

In order for a mushy layer to form, compositional undercooling must manifest. Following Worster (1986), the condition for constitutional undercooling to occur is taken as

$$\boldsymbol{n} \cdot \bar{\boldsymbol{\nabla}} T < \Gamma \boldsymbol{n} \cdot \bar{\boldsymbol{\nabla}} C, \tag{2.4}$$

where $\boldsymbol{n}$ is a unit vector normal to the solidification front.

The melt ampoule is taken to be a semi-infinite domain described by Cartesian coordinates $\bar{\boldsymbol{x}} = (\bar{x}, \bar{y}, \bar{z})$ with corresponding unit vectors $(\boldsymbol{e}_x, \boldsymbol{e}_y, \boldsymbol{e}_z)$ with $\boldsymbol{e}_z$ anti-parallel to the gravity vector $\boldsymbol{g}$. The system solidifies at a constant rate $V$ and the solid-mush interface can be located at $\bar{z} = 0$ in a frame moving with the solidification front. The height of the mushy zone is $\bar{h}(\bar{x}, \bar{y}, \bar{t})$.

At the solid-mush interface, $\bar{z} = 0$, the temperature is held at the eutectic temperature and no penetration of fluid into the solid region is possible:

$$T = T_\mathrm{E}, \quad \bar{\boldsymbol{u}} \cdot \boldsymbol{e}_z = 0, \tag{2.5}$$

where $\bar{\boldsymbol{u}}$ is the velocity vector. We assume that the mush is in local thermodynamic equilibrium. When the mushy layer is in local thermodynamic equilibrium, the temperature and composition are related by the liquidus curve on the phase diagram, described by (2.1) throughout the layer.

Typically the length scale of the dendritic structures is much smaller than other length scales in the problem, therefore the mush is treated as a single homogenous continuum consisting of solid and liquid phases (Batchelor 1994). The heat and molecular mass transport properties of the mushy region are taken to be volume-weighted averages of the two phases, expressed using the volume fraction of liquid, $\hat{\chi}$, as

$$k_\mathrm{m} = \hat{\chi} k_\mathrm{l} + (1 - \hat{\chi})\, k_\mathrm{s} \tag{2.6}$$

$$D_\mathrm{m} = \hat{\chi} D_\mathrm{l} + (1 - \hat{\chi})\, D_\mathrm{s} \tag{2.7}$$

Similarly, the specific heat per unit volume is

$$c_\mathrm{m} = \hat{\chi} c_\mathrm{l} + (1 - \hat{\chi})\, c_\mathrm{s} \tag{2.8}$$

$c_\mathrm{s}, c_\mathrm{l}$ are the specific heats per unit volume of the solid and the fluid parts of the mush.

We then model the mushy layer as a porous medium where Darcy's law holds, following Roberts & Loper (1983), Fowler (1985),and Worster (1992). When the Oberbeck-Boussinesq approximation is applied conservation of mass, momentum, heat and species

may be written

$$\frac{\nu}{\Pi(\hat{\chi})}\bar{\boldsymbol{u}} = -\bar{\boldsymbol{\nabla}}\left(\frac{p}{\rho}\right) + \left(\frac{\rho}{\rho_0} - 1\right)\boldsymbol{g} \tag{2.9a}$$

$$\bar{\boldsymbol{\nabla}} \cdot \bar{\boldsymbol{u}} = 0, \tag{2.9b}$$

$$c_{\mathrm{m}}\left(\frac{\partial}{\partial \bar{t}} - V\frac{\partial}{\partial \bar{z}}\right)T + c_{\mathrm{l}}\bar{\boldsymbol{u}} \cdot \bar{\boldsymbol{\nabla}}T = \bar{\boldsymbol{\nabla}} \cdot \left(k_{\mathrm{m}}\bar{\boldsymbol{\nabla}}T\right) - L\left(\frac{\partial}{\partial \bar{t}} - V\frac{\partial}{\partial \bar{z}}\right)\hat{\chi}, \tag{2.9c}$$

$$\left(\frac{\partial}{\partial \bar{t}} - V\frac{\partial}{\partial \bar{z}}\right)\left[\hat{\chi}C + (1-\hat{\chi})\,C_{\mathrm{s}}\right] + \bar{\boldsymbol{u}} \cdot \bar{\boldsymbol{\nabla}}C = \bar{\boldsymbol{\nabla}} \cdot \left(D_{\mathrm{m}}\bar{\boldsymbol{\nabla}}C\right) \tag{2.9d}$$

Here $p = p^*/\rho_0 - \boldsymbol{g} \cdot \bar{\boldsymbol{x}}$ is the pressure,$L$ is the latent heat of solidification.

The model of the solidifying mushy layer described up to this point is similar to models considered in many previous studies. The differences between these models come from assumptions about the size of the mushy layer and the boundary conditions at the mush-liquid interface. Worster (1992) considered the liquid region above the mushy layer to be a semi-infinite region modeled as an extended Boussinesq fluid (Hills *et al.* 1983). The extent of the mushy layer was determined by the definition $\hat{\chi} = 1$ and the assumption that the mush-liquid system adopts a state of marginal thermodynamic equilibrium, proposed by Worster (1986). For a mushy layer to manifest, constitutional supercooling must occur. If the gradient of the temperature is equal to the liquidus temperature gradient in the liquid immediately adjacent to the mushy zone, then dendrites cannot exist above that point, and the thickness of the mushy layer is dictated by the condition

$$\boldsymbol{n} \cdot \bar{\boldsymbol{\nabla}}T = \Gamma \boldsymbol{n} \cdot \bar{\boldsymbol{\nabla}}C. \tag{2.10}$$

In the two layer model, the mush-liquid interface is treated as a free surface, where heat and solute are conserved

$$L[\![\hat{\chi}]\!]V = [\![k_{\mathrm{m}}\boldsymbol{n} \cdot \bar{\boldsymbol{\nabla}}T]\!] \tag{2.11}$$

$$(C - C_{\mathrm{s}})\,[\![\hat{\chi}]\!]V = [\![D_{\mathrm{m}}\boldsymbol{n} \cdot \bar{\boldsymbol{\nabla}}C]\!]. \tag{2.12}$$

The continuity of mass flux, pressure, temperature, and heat flux at the surface leads to the following interfacial jump conditions,

$$[\![\boldsymbol{n} \cdot \bar{\boldsymbol{u}}]\!] = 0, \quad [\![p]\!] = 0, \quad [\![T]\!] = 0, \quad [\![\boldsymbol{n} \cdot \bar{\boldsymbol{\nabla}}T]\!] = 0 \tag{2.13}$$

At the mush-liquid interface $\bar{z} = \bar{h}(\bar{x}, \bar{y}, \bar{t})$, it is assumed that there is no slip,

$$\bar{\boldsymbol{u}} - \boldsymbol{n} \cdot \bar{\boldsymbol{u}} = 0 \tag{2.14}$$

and that the temperature is on the liquidus

$$T = T_{\mathrm{L}}\left(C_0\right) + \Gamma\left(C - C_0\right). \tag{2.15}$$

Amberg & Homsy (1993) and many subsequent papers take a simpler approach. Rather than explicitly modeling both the liquid and mushy layers, they focus on the mushy layer only. The conditions at the solid-mush interface and the condition that $\hat{\chi} = 1$ at the mush-liquid interface are retained. However, they introduce the depth of the mushy layer as a distinct length scale. In order to obtain a system that is tractible by purely analytical means, they assume that the mushy layer depth is small. To further simplify their analysis, they chose a condition that the mush-layer interface is impermeable to flow.

$$\bar{\boldsymbol{u}} \cdot \boldsymbol{n} = 0 \qquad \text{at} \quad \bar{z} = \bar{h}. \tag{2.16}$$

This choice results in a decoupling of the superposed liquid layer from the mushy zone. To close the system, they set the temperature at $\bar{z} = \bar{h}$ to

$$T = T_{\mathrm{L}}(C_0). \tag{2.17}$$

Chung & Chen (2000) considered the Amberg-Homsy model with one modification. Instead of considering the mush-liquid interface to be impermeable and using (2.16), they considered the mush and liquid to be coupled following Emms & Fowler (1994). A constant pressure condition was used that leads to a vanishing vertical gradient of the vertical velocity,

$$\boldsymbol{n} \cdot \bar{\boldsymbol{\nabla}}(\bar{\boldsymbol{u}} \cdot \boldsymbol{n}) = 0 \qquad \text{at} \quad \bar{z} = \bar{h}. \tag{2.18}$$

Chung and Chen reported quantitative improvements over the Amberg-Homsy model and better agreement with linear results of the two-layer system.

A hybrid of the single- and double-layer approaches is developed into the model presented here. We retain the decoupling of the liquid and mushy regions, so that only the mushy region is considered. However, we presuppose the existence of the liquid region above and apply the condition of marginal thermodynamic equilibrium to obtain the mushy layer thickness in terms of the characteristic length due to thermal diffusion. This approach has been taken for studying linear stability in the two-layer model (Worster 1992; Chen *et al.* 1994). The models of Amberg-Homsy and Chung-Chen differ by a single boundary condition. The Chung-Chen model appears to be a more physical formulation, however a larger body of research exists using the Amberg-Homsy model. We analyze both cases and write the dynamic boundary conditions at the mush-liquid interface to be either (2.16) or (2.18).

### 2.2. *Non-dimensional system*

The governing equations are non-dimensionalized by using $V$, $\kappa/V$, $\kappa/V^2$, $\Delta C$, $[(\beta^* - \Gamma\alpha^*)\Delta C\,\rho_0 g\kappa]/V$ and $\Delta T$ as scales for velocity, length, time, solute, pressure and temperature, respectively. Here $\kappa$ is the thermal diffusivity, $\rho_0$ is a constant reference density, $\beta = \beta^* - \Gamma\alpha^*$, $\Delta C = C_0 - C_{\mathrm{E}}$ and $\Delta T = T_L(C_0) - T_{\mathrm{E}}$. The non-dimensional form of the equations for momentum, continuity, temperature and solute concentration derived from (2.9) are then

$$\hat{K}(\hat{\chi})\hat{\boldsymbol{u}} = -\boldsymbol{\nabla}\hat{p} - \mathscr{R}_{\mathrm{m}}\hat{\theta}\boldsymbol{e}_z \tag{2.19a}$$

$$\boldsymbol{\nabla} \cdot \hat{\boldsymbol{u}} = 0, \tag{2.19b}$$

$$\left(\tfrac{\partial}{\partial t} - \tfrac{\partial}{\partial z}\right)\left[\hat{\theta} - \mathscr{S}(1-\hat{\chi})\right] + \hat{\boldsymbol{u}} \cdot \boldsymbol{\nabla}\hat{\theta} = \triangle\hat{\theta} \tag{2.19c}$$

$$\left(\tfrac{\partial}{\partial t} - \tfrac{\partial}{\partial z}\right)\left[\hat{\chi}\hat{\theta} + \mathscr{C}(1-\hat{\chi})\right] + \hat{\boldsymbol{u}} \cdot \boldsymbol{\nabla}\hat{\theta} = \varepsilon_{\mathrm{m}}\boldsymbol{\nabla} \cdot \hat{\chi}\boldsymbol{\nabla}\hat{\theta} \tag{2.19d}$$

where $\hat{\boldsymbol{u}} = \hat{u}\boldsymbol{e}_x + \hat{v}\boldsymbol{e}_y + \hat{w}\boldsymbol{e}_z$ is the volume flux per unit area, which is also known as the Darcy velocity vector (Nield 1998);$\hat{u}$ and $\hat{v}$ are the horizontal components of $\hat{\boldsymbol{u}}$ along $x$- and $y$-directions, respectively; $\hat{w}$ is the vertical component of $\hat{\boldsymbol{u}}$ along the $z$-direction; $\hat{p}$ is the modified pressure; $\hat{\theta}$ is the non-dimensional composition, or equivalently temperature (Worster 1992), $\hat{\theta} = [T - T_L(C_0)]/\Delta T = (C - C_0)/\Delta C$; $t$ is the time variable; $\hat{\chi}$ is the local liquid fraction or porosity; $\mathcal{R} = \beta\Delta C g \Pi(1)/(V\nu)$ is the Rayleigh number, $\Pi(0)$ is a reference value at $\hat{\chi} = 0$ of the permeability $\Pi(\hat{\chi})$ of the porous medium, which is assumed to be finite (Worster 1992), $\nu$ is the kinematic viscosity, $g = |\boldsymbol{g}|$ is acceleration due to gravity; $K(\hat{\chi}) = \Pi(0)/\Pi(\hat{\chi})$, $\varepsilon_{\mathrm{m}} = D_{\mathrm{m}}/\kappa$ is the inverse of the Lewis number; $\mathscr{S} = L/(C_{\mathrm{m}}\Delta T)$ is the Stefan number, $C_{\mathrm{m}}$ is the specific heat per unit volume, $L$ is the latent heat of solidification per unit volume; $\mathscr{C} = (C_{\mathrm{s}} - C_0)/\Delta C$ is a concentration

ratio and $C_s$ is the composition of the solid-phase forming the dendrites. We assume that temperature equilibrates much faster than mass, so that $\varepsilon_m = 0$ for all analyses and results herein.

The governing equations (2.19) are subject to the following boundary conditions:

$$\hat{\theta} = -1, \quad \hat{w} = 0 \qquad \text{at } z = 0 \tag{2.20a,b}$$

$$\hat{\theta} = 0, \qquad \hat{w} = 0 \quad \text{or} \quad \frac{\partial}{\partial z}\hat{w} = 0, \quad \hat{\chi} = 1 \quad \text{at } z = \delta, \tag{2.20c–e}$$

where $\delta$ represents the dimensionless depth of the layer.

The permeability relation is

$$\hat{K}(x, y, z, t) = \frac{\Pi(1)}{\Pi(\hat{\chi})}$$

and the permeability $\Pi$ is derived from

$$\Pi = \hat{\chi}^J(x, y, z, t)$$

to obtain

$$\hat{K} = \hat{\chi}^{-J} \tag{2.21}$$

Generally, $\hat{K}$ will decrease as $\hat{\chi}$ increases. Setting $J = 0$ correspondes to a constant permeability and represents a passive mushy layer with no coupling between permeability and porosity. When $J = 3$, equation (2.21) resembles a Kozeny-type equation for permeability in which the specific volumetric surface area of the phase boundaries is considered constant (Lage 1998). These two relations for $\hat{K}$ has been used by many authors (Worster 1992; Amberg & Homsy 1993; Emms & Fowler 1994) in similar studies.

## 3. Analyses

Usually the assumption of a thin mushy layer ($\delta \ll 1$) and an initial composition that is close to the eutectic composition are employed to render an analytically tractable system. In such systems, in particular, the basic-state solution is expressed in terms of asymptotic expansions in $\delta$ and perturbations at each order $\epsilon$ are expanded asymptotically in terms of $\delta$. Usually either a distinguished limit $\delta = O(\epsilon)$ or double-limit where $\delta = O(1)$ as $\epsilon \to 0$ is chosen yielding complicated, though analytical, expressions. Here an alternative approach is taken. If the constraint of analytical solutions is removed and the use of one-dimensional numerical methods is accepted, then the governing system may be studied in parameter regimes beyond those accessible by previous analyses.

### 3.1. *Steady basic-state and perturbation systems*

The perturbation from the basic state is measured by the amplitude $\epsilon$,

$$\hat{\theta} = \theta_b(z) + \epsilon\theta(x, y, z, t), \tag{3.1a}$$

$$\hat{\chi} = \chi_b(z) + \epsilon\chi(x, y, z, t), \tag{3.1b}$$

$$\hat{\boldsymbol{u}} = 0 + \epsilon\boldsymbol{u}(x, y, z, t), \tag{3.1c}$$

$$\hat{p} = p_b(z) + \epsilon p(x, y, z, t), \tag{3.1d}$$

$$\hat{K} = K_b(\chi_b) + \epsilon K(\chi). \tag{3.1e}$$

The perturbation is the small deviation of each dependent variable from its basic quantity. This deviation can vary with respect to spatial and time variables, as is shown in (3.1).

As in Worster (1991), substituting the expressions (3.1) into (2.19), we obtain the

equations governing the steady basic state:

$$\frac{\mathrm{d}^2\theta_b}{\mathrm{d}z^2}+\frac{\mathrm{d}\theta_b}{\mathrm{d}z}+\mathscr{S}\frac{\mathrm{d}\chi_b}{\mathrm{d}z}=0, \qquad \chi_b\frac{\mathrm{d}\theta_b}{\mathrm{d}z}+(\theta_b-\mathscr{C})\frac{\mathrm{d}\chi_b}{\mathrm{d}z}=0$$

$$\theta_b=-1 \text{ at } z=0, \qquad \theta_b=0,\ \chi_b=1 \text{ at } z=\delta.$$

From consideration of the melt region above the mush, we obtain the following solutions for the basic state. We can integrate the heat equation once, then substitute the expression for $\varphi_b$ into it, and integrate again to obtain the following relationship between $z$ and $\theta_b$:

$$z(\theta_b)=\frac{a_1-\mathscr{C}}{a_1-a_2}\ln\left(\frac{1+a_1}{a_1-\theta_b}\right)+\frac{(\mathscr{C}-a_2)}{a_1-a_2}\ln\left(\frac{1+a_2}{a_2-\theta_b}\right) \tag{3.2}$$

where

$$a_1,a_2=\frac{1}{2}\left[(\mathscr{S}+\mathscr{C}+\theta_\infty)\pm\sqrt{(\mathscr{S}+\mathscr{C}+\theta_\infty)^2-4\mathscr{C}\theta_\infty}\right]$$

and

$$\chi_b=\frac{\mathscr{C}}{\mathscr{C}-\theta_b} \tag{3.3}$$

The thickness of the mushy layer, $\delta$, is obtained from the system parameters $\mathscr{C}, \mathscr{S}$ and $\theta_\infty$ by

$$\delta=\frac{a_1-\mathscr{C}}{a_1-a_2}\ln\left(\frac{1+a_1}{a_1}\right)+\frac{(\mathscr{C}-a_2)}{a_1-a_2}\ln\left(\frac{1+a_2}{a_2}\right) \tag{3.4}$$

In previous nonlinear analyses, the assumption of a thin mushy layer $\delta\ll 1$ leads to basic-state solutions in terms of asymptotic expansions. In such circumstances, the perturbations to liquid fraction are small $\chi\ll 1$ and the permeability factor $K$ is expanded in a Taylor series about $\chi=0$. To consider larger mushy layer thicknesses, we need to model the effect of porosity on permeability. A common choice following from the Kozeny equation is (2.21) for $J>0$. Using (3.1$e$) in (2.21), we have

$$K_b=\chi_b^{-J}, \tag{3.5}$$

$$K\sim -J\chi_b^{-(J+1)}\left(\chi-\epsilon\tfrac{J+1}{2}\chi_b^{-1}\chi^2\right). \tag{3.6}$$

For analysis of the perturbation system to be presented in this section, it is convenient to use the general representation

$$\boldsymbol{u}=\boldsymbol{\Omega}P+\boldsymbol{E}\psi, \tag{3.7}$$

$$\boldsymbol{\Omega}\equiv\boldsymbol{\nabla}\times\boldsymbol{\nabla}\times\boldsymbol{e}_z, \quad \boldsymbol{E}\equiv\boldsymbol{\nabla}\times\boldsymbol{e}_z, \tag{3.8}$$

for the divergence-free vector field $\boldsymbol{u}$ (Chandrasekar 1981). Here $P$ and $\psi$ are the poloidal and toroidal functions for $\boldsymbol{u}$, respectively. By taking the vertical component of the curl of (2.19$a$), it can be shown that the toroidal part $\boldsymbol{E}\psi$ of $\boldsymbol{u}$ must vanish. Taking the vertical components of the double curl of (2.19$a$) and using (2.19$b$) in (2.19)–(2.20), we find the following system, which will be analyzed in this section:

$$(K_b\triangle+K_b'\tfrac{\partial}{\partial z})\triangle_2P-\mathscr{R}_{\mathrm{m}}\triangle_2\theta=-\epsilon\left[\tfrac{\partial}{\partial z}\left(\boldsymbol{\nabla}K\cdot\boldsymbol{\Omega}P\right)+\triangle\left(K\triangle_2P\right)\right], \tag{3.9$a$}$$

$$\left(\tfrac{\partial}{\partial t}-\tfrac{\partial}{\partial z}-\triangle\right)\theta+\mathscr{S}\left(\tfrac{\partial}{\partial t}-\tfrac{\partial}{\partial z}\right)\chi-\theta_b'\triangle_2P=-\epsilon\boldsymbol{\Omega}P\cdot\boldsymbol{\nabla}\theta, \tag{3.9$b$}$$

$$\begin{aligned}\left[\chi_b(\tfrac{\partial}{\partial t}-\tfrac{\partial}{\partial z})-\chi_b'\right]\theta-\left[(\theta_b-\mathscr{C})(\tfrac{\partial}{\partial t}-\tfrac{\partial}{\partial z})-\theta_b'\right]\chi-\theta_b'\triangle_2P\\ =-\epsilon\left[\boldsymbol{\Omega}P\cdot\boldsymbol{\nabla}\theta+\chi\left(\tfrac{\partial}{\partial t}-\tfrac{\partial}{\partial z}\right)\theta+\theta\left(\tfrac{\partial}{\partial t}-\tfrac{\partial}{\partial z}\right)\chi\right],\end{aligned} \tag{3.9$c$}$$

$$\theta = 0, \quad P = 0 \qquad\qquad\qquad\qquad \text{at } z = 0 \qquad\qquad (3.10a,b)$$

$$\theta = 0, \quad P = 0 \quad \text{or} \quad \tfrac{\partial}{\partial z}P = 0, \quad \chi = 0 \quad \text{at } z = \delta \qquad\qquad (3.10c\text{–}e)$$

where

$$\triangle_2 \equiv \partial^2/\partial x^2 + \partial^2/\partial y^2.$$

It will be useful to define the notation $\boldsymbol{q} = (\theta, \chi, P)^{\mathrm{T}}$ and introduce the multilinear operators $\boldsymbol{\mathcal{L}}, \hat{\boldsymbol{\mathcal{L}}}$ and $\boldsymbol{\mathcal{N}}$, defined by (A 1)–(A 3) in the appendix, to represent the perturbation equations (3.9) succinctly as

$$(\boldsymbol{\mathcal{L}} - \mathscr{R}_{\mathrm{m}}\hat{\boldsymbol{\mathcal{L}}})\boldsymbol{q} = \epsilon\boldsymbol{\mathcal{N}}(\boldsymbol{q}, \boldsymbol{q}). \qquad (3.11)$$

The boundary conditions (3.10) are represented generally as

$$\boldsymbol{\mathcal{B}}\left[\boldsymbol{q}(z = 0), \boldsymbol{q}(z = \delta)\right] = 0 \qquad (3.12)$$

### 3.2. *Linear stability analysis*

To investigate the stability of the basic state to arbitrary infinitesimal perturbations, the perturbation system is linearized. Designating the linear solution by $\boldsymbol{q}_0$ and setting $\epsilon = 0$ in (3.11)–(3.12), we find the linear system for the perturbations

$$\left(\boldsymbol{\mathcal{L}} - \mathscr{R}_{\mathrm{m}}\hat{\boldsymbol{\mathcal{L}}}\right)\boldsymbol{q}_0 = 0, \quad \boldsymbol{\mathcal{B}}_0\left[\boldsymbol{q}_0(z = 0), \boldsymbol{q}_0(z = \delta)\right] = 0. \qquad (3.13a)$$

Since the coefficients in (3.13) are functions of $z$ only, the method of separation of variables is applicable to obtain the solution. Using normal mode analysis (Chandrasekar 1981), the perturbations are expressed in terms of a complete set of normal modes in the form of two-dimensional waves. We consider disturbances of the form

$$\boldsymbol{q}_0 = \tilde{\boldsymbol{q}}_0(z)H(x, y)\exp(\sigma t) \qquad (3.14)$$

where $\sigma$ is the growth rate of the perturbations and the function $H(x, y)$ satisfies

$$\triangle_2 H = -\alpha^2 H. \qquad (3.15)$$

Many flows of interest may be described by periodic cells in the horizontal directions. In such cases, the planform function $H$ is given by

$$H(x, y) = \textstyle\sum_{n=-N}^{N} A_n H_n, \quad H_n \equiv \exp\left(\mathrm{i}\boldsymbol{\alpha}_n \cdot \boldsymbol{x}\right), \qquad (3.16)$$

where $N$ is a positive integer, $\alpha_n$ are the horizontal wavenumber vectors satisfying

$$\boldsymbol{\alpha}_n \cdot \boldsymbol{e}_z = 0, \qquad |\boldsymbol{\alpha}_n| = \alpha, \qquad \boldsymbol{\alpha}_{-n} = -\boldsymbol{\alpha}_n \qquad (3.17)$$

and the constant coefficients $A_n$ satisfy the conditions

$$\textstyle\sum_{n=-N}^{N} A_n A_n^* = 1, \qquad A_{-n} = A_n^* \qquad (3.18)$$

where the asterisk indicates complex conjugation. The $z$-dependent coefficient $\tilde{\boldsymbol{q}}_0$ in (3.14) satisfies a system of the form (3.13), when $\partial/\partial t, \partial/\partial z, \mathscr{R}_{\mathrm{m}}, \triangle_2$, and $\triangle$ in $\boldsymbol{\mathcal{L}}$ and $\hat{\boldsymbol{\mathcal{L}}}$ are replaced, respectively, by $\sigma, \mathrm{D} \equiv \mathrm{d}/\mathrm{d}z, R_0, -\alpha^2$, and $(\mathrm{D}^2 - \alpha^2)$, where $R_0$ is defined in the next paragraph.

For each wavenumber $\alpha$, a marginal Rayleigh number $\mathscr{R}_{\mathrm{m}}$ is computed at which $\sigma = 0$. The result may be plotted to obtain a marginal stability curve. The least stable mode corresponds to the minimum Rayleigh number and wavenumber $\alpha_c$ on this curve. To simplify notation, the minimum marginal Rayleigh number and corresponding critical wavenumber are henceforth denoted as $R_0$ and $\alpha$, respectively.

### 3.3. *Nonlinear analysis*

#### 3.3.1. *Adjoint System*

In order to compute solvability conditions, the solutions to the adjoint linear problem are required. Many authors put the equations in self-adjoint form, however we take the more general approach of computing adjoint solutions. When solutions to (3.13) have the form of (3.14), the adjoint identity yields adjoint solutions of the form

$$\boldsymbol{q}_{0n}^{(\mathrm{a})} = [\theta_{0n}^{(\mathrm{a})}, \chi_{0n}^{(\mathrm{a})}, P_{0n}^{(\mathrm{a})}] = [\tilde{\theta}_0^{(\mathrm{a})}(z), \tilde{\chi}_0^{(\mathrm{a})}(z), \tilde{P}_0^{(\mathrm{a})}(z)] A_n H_n(x,y) \tag{3.19}$$

where the $z$-dependent coefficient function $\tilde{\boldsymbol{q}}_{0n}^{(\mathrm{a})} = [\tilde{\theta}_0^{(\mathrm{a})}(z), \tilde{\chi}_0^{(\mathrm{a})}(z), \tilde{P}_0^{(\mathrm{a})}(z)]$ are the solutions of the linear system

$$\mathbf{L}^{(\mathrm{a})} \tilde{\boldsymbol{q}}_0^{(\mathrm{a})} = 0, \qquad \mathbf{B}^{(\mathrm{a})}[\tilde{\boldsymbol{q}}_0^{(\mathrm{a})}(z=0), \tilde{\boldsymbol{q}}_0^{(\mathrm{a})}(z=\delta)] = 0. \tag{3.20}$$

The linear operator $\mathbf{L}^{(\mathrm{a})}$ and the boudary conditions represented by $\mathbf{B}^{(\mathrm{a})}$ are defined by (A 4) in the appendix.

#### 3.3.2. *Expansions*

:q The following expansions are made for the perturbation quantities needed in the present analysis up to order $\epsilon^2$:

$$(P, \theta, \chi, \mathscr{R}_{\mathrm{m}}) \sim \textstyle\sum_{n=0}^{2} (P_n, \theta_n, \chi_n, R_n)\, \epsilon^n \tag{3.21}$$

It should also be noted that in the present analyses, we have used the following expansion for $K$ up to order $\epsilon$

$$K \sim K_0 + \epsilon K_1, \tag{3.22}$$

where it was found from (3.6) that

$$K_0 = -J \chi_b^{-(J+1)} \chi_0, \tag{3.23a}$$

$$K_1 = -J \chi_b^{-(J+1)} \left( \chi_1 - \tfrac{J+1}{2} \chi_b^{-1} \chi_0^2 \right). \tag{3.23b}$$

#### 3.3.3. *First Order Problem*

At $O(\epsilon)$, the first order perturbation problem is found from (3.11)–(3.12) to be

$$(\boldsymbol{\mathcal{L}} - R_0 \hat{\boldsymbol{\mathcal{L}}}) \boldsymbol{q}_1 = R_1 \hat{\boldsymbol{\mathcal{L}}} \boldsymbol{q}_0 + \boldsymbol{\mathcal{N}}(\boldsymbol{q}_0, \boldsymbol{q}_0) \tag{3.24a}$$

$$\boldsymbol{\mathcal{B}}_0 [\boldsymbol{q}_0(z=0), \boldsymbol{q}_0(z=\delta)] = 0. \tag{3.24b}$$

when the linear solution (3.14) is used in the right-hand-side of (3.24$a$) and some simplifications are made, we find

$$(\boldsymbol{\mathcal{L}} - R_0 \hat{\boldsymbol{\mathcal{L}}}) \boldsymbol{q}_1 = R_1 \widehat{\mathbf{L}}(\alpha) \tilde{\boldsymbol{q}}_0 \sum_{n=-N}^{N} A_n H_n + \sum_{k,p=-N}^{N} \widetilde{\mathbf{N}}_{10}(\Phi_{lp}; z) A_k A_p H_k H_p \tag{3.25}$$

where the matrix $\widehat{\mathbf{L}}(\alpha)$ has the same form as $\hat{\boldsymbol{\mathcal{L}}}$ given by (A 2) with $\triangle_2$ replaced by $-\alpha^2$ and the vector function $\widetilde{\mathbf{N}}_{10}$ is given by (A 5) in the appendix.

The double sum over $k$ and $p$ has $(2N)^2$ terms, however symmetries exist which simplify the expression. First, the $H_k H_p$ terms are symmetric, $H_k H_p = H_p H_k$, bringing the number of independent pairs of $H$ to $N(2N+1)$. Sums also involve the parameter $\Phi_{kp} = \boldsymbol{\alpha}_k \cdot \boldsymbol{\alpha}_p / \alpha^2$. This parameters has the properties

$$\Phi_{kp} = \Phi_{pk}, \quad \Phi_{kp} = \Phi_{-k,-p}, \quad \Phi_{k,-p} = -\Phi_{kp}, \quad \Phi_{kk} = 1 \tag{3.26}$$

Of the $N(2N+1)$ terms, there are $2N$ terms associated with $\Phi_{kk} = 1$, $N$ terms associated

with $\Phi_{k,-k} = -1$. If $k \neq p$, then $\Phi_{k,-p} = -\Phi_{lp}$ implies that there are only $N$ possible independent $\Phi$ quantities. There are two case independent $\Phi$'s for $N = 2$, but in the regular case of square cells they are both zero and therefore not distinct. In the regular solution for $N = 3$, corresponding to hexagonal cells, only two $\Phi$'s are possible. In summary, for the convection patterns considered here: $\Phi_{kp} = \pm 1$ for rolls, $\Phi_{kp} = \pm 1, \pm\cos\gamma$ for rectangles, $\Phi_{kp} = \pm 1, 0$ for squares and $\Phi_{kp} = \pm 1, \pm 1/2$ for hexagons.

The linear system (3.13) has non-trivial solutions, and for (3.24) to be solvable, the non-homogenous term must be orthogonal to the solution of the adjoint linear system. This condition is given by

$$\langle \boldsymbol{q}_{0n}^{(\mathrm{a})}, R_1 \hat{\boldsymbol{\mathcal{L}}} \boldsymbol{q}_0 + \boldsymbol{\mathcal{N}}(\boldsymbol{q}_0, \boldsymbol{q}_0) \rangle = 0, \tag{3.27}$$

where the angular bracket indicates integration over the whole fluid layer. From this condition, we find that $R_1 = 0$ except for the case of hexagonal cells ($N = 3$):

$$R_1 = -\frac{2\langle \tilde{\boldsymbol{q}}_0^{(\mathrm{a})}, \widetilde{\mathbf{N}}_{10}(-1/2; z) \rangle}{\sqrt{6}\langle \tilde{P}_0^{(\mathrm{a})}, K_b^{-1}\tilde{\theta}_0 \rangle}. \tag{3.28}$$

The solution to (3.24) is found to be of the form

$$\boldsymbol{q}_1(x, y, z) = \tilde{\boldsymbol{q}}_{10}(z) \sum_{n=-N}^{N} A_n H_n + \sum_{k,p=-N}^{N} \tilde{\boldsymbol{q}}_{11}(\Phi_{kp}; z) A_k A_p H_k H_p, \tag{3.29}$$

where the boundary value problems for the $z$-dependent coefficients $\tilde{\boldsymbol{q}}_{10}$ and $\tilde{\boldsymbol{q}}_{11}$ are given by (A 8) in the appendix.

3.3.4. *Second Order Problem*

We now consider the system (3.11)–(3.12) at order $\epsilon^2$. The second order perturbation problem is then

$$(\boldsymbol{\mathcal{L}} - R_0\hat{\boldsymbol{\mathcal{L}}})\boldsymbol{q}_2 = R_1\hat{\boldsymbol{\mathcal{L}}}\boldsymbol{q}_1 + R_2\hat{\boldsymbol{\mathcal{L}}}\boldsymbol{q}_0 + \boldsymbol{\mathcal{N}}(\boldsymbol{q}_0, \boldsymbol{q}_1) + \boldsymbol{\mathcal{N}}(\boldsymbol{q}_1, \boldsymbol{q}_0) \tag{3.30}$$

$$\boldsymbol{\mathcal{B}}[\boldsymbol{q}_2(z = 0), \boldsymbol{q}_2(z = \delta)] = 0. \tag{3.31}$$

The solvability condition at this order yields the expression for $R_2$,

$$R_2 = \frac{-R_1\langle \boldsymbol{q}_{0n}^{(\mathrm{a})}, \hat{\boldsymbol{\mathcal{L}}}\boldsymbol{q}_1 \rangle + \langle \boldsymbol{q}_{0n}^{(\mathrm{a})}, \boldsymbol{\mathcal{N}}(\boldsymbol{q}_0, \boldsymbol{q}_1) + \boldsymbol{\mathcal{N}}(\boldsymbol{q}_1, \boldsymbol{q}_0) \rangle}{\langle \boldsymbol{q}_{0n}^{(\mathrm{a})}, \hat{\boldsymbol{\mathcal{L}}}\boldsymbol{q}_0 \rangle} \tag{3.32}$$

The system (3.30), together with (3.18) and (3.28), can be used to study the steady solutions in the form of two-dimensional rolls and three-dimensional cells. We shall restrict our attention to the simplest types of solutions, which include those observed in the applications. These solutions are called regular or semi-regular solutions (Busse 1967). In the case of a regular solution all angles between two neighboring $\boldsymbol{\alpha}$-vectors are equal and (3.18) yields

$$|A_1|^2 = \cdots = |A_N|^2 = \tfrac{1}{2N} \tag{3.33}$$

In the more general semi-regular solution, where (3.33) still holds, the scalar products between any of the $\boldsymbol{\alpha}$-vectors and its two neighboring $\boldsymbol{\alpha}$-vectors assume the constant values $\alpha_1$ and $\alpha_2$. An example of a semi-regular solution is that due to rectangular cells ($N = 2$), where $\alpha_1 = -\alpha_2$. Regular solutions can follow from the semi-regular ones for the special case $\alpha_1 = \alpha_2$. Simple forms of regular solutions correspond to the cases of two-dimensional rolls ($N = 1$), square cells ($N = 2$) and hexagons ($N = 3$).

The simplest types of solutions, which turn out to be preferred under certain conditions

in the present study, are described briefly as follows. For steady two-dimensional rolls, $N = 1$, $A_n = 1/2$ and $R_1 = 0$. For rectangular pattern convection, $N = 2$, $A_n = 1/2, \gamma \neq 90^\circ$ and $R_1 = 0$. Here $\gamma$ is the angle ($\gamma \leqslant 90^\circ$) between two adjacent wavenumber vectors of any cell. For square pattern convection, $N = 2$, $A_n = 1/2, \gamma = 90^\circ$ and $R_1 = 0$. For hexagonal convection, $N = 3$, $A_n = 1/6$ and $R_1 \neq 0$ in general (Busse 1978). As will be referred to later in sections 4 and 5, the sign of the vertical motion at the cells' centers for hexagons, which is determined by the sign of $\epsilon$, is inferred from the condition

$$\epsilon R_1 < 0 \tag{3.34}$$

for the subcritical hexagons at order $\epsilon$ and from

$$\epsilon R_1 > 0 \tag{3.35}$$

for the supercritical hexagons at order $\epsilon$. If the sign of the vertical motion at the cells' centers for the hexagons is negative, such hexagons are referred to as down-hexagons, while up-hexagons are referred to the case where the sign of the vertical motion is positive at the cells' centers.

### 3.4. *Computation*

#### 3.4.1. *Marginal stability problem*

In contrast with previous studies of nonlinear convection in mushy layers, discussed in section 1, the equations for determining linear stability must be solved numerically. To determine linear stability, we use a shooting technique (Keller 1976). For a given set of parameters, linear modes are integrated across the domain of the mush and the Rayleigh number is varied until boundary conditions are satisfied. By computing this neutral Rayleigh number for a range of wavenumbers, we produce a marginal stability curve. The minimum value of $R_0$ with respect to $\alpha$ is then determined from the marginally stable states for different wavenumbers. The associated solutions $\tilde{\boldsymbol{q}}_0$ at that critical Rayleigh number are the eigenfunctions of the linear system.

We follow Worster (1992) and use the basic-state temperature as the independent variable in the linear disturbance equations to avoid having to invert the transcendental equation (3.2). The variable

$$\tau = -\theta_b \tag{3.36}$$

maps the computational domain of the mushy zone to $[0, 1]$. In this mapping, $\tau = 0$ corresponds to the mush-liquid interface and the solid-mush interface is located at $\tau = 1$. The set of ordinary differential equations for $\tilde{\boldsymbol{q}}_0(z)$ is converted to the corresponding system with $\tau$ as the independent variable prior to employing the shooting method.

#### 3.4.2. *Nonlinear problem*

Once the minimum Rayleigh number and corresponding wavenumber are found from the marginal stability problem, we solve the adjoint problem in $\tau$. We checked the numerical integrity of the adjoint solutions by generating a neutral curve from the adjoint system. The validity was ensured when a neutral curve generated by the same technique described before for the marginal stability problem, but using the adjoint system instead of the linear system, was computed and found to be equal to the linear neutral curve. Once the adjoint solutions are found, we use (3.36) to convert the nonhomogeneous linear system in $z$ at each order $\epsilon$ into a system with independent variable $\tau$.

For the higher perturbation orders considered, $\epsilon$ and $\epsilon^2$, the solvability conditions (3.28) and (3.32) were applied to yield higher order corrections to the Rayleigh number. After calculating $R_1$ using numerical integration over the $\tau$-grid, the $O(\epsilon)$ perturbation

modes were computed. For each independent constituent perturbation mode, $\Phi_{lp}$, associated with each convection pattern considered, a vertical mode was computed from systems ordinary differential equations and boundary conditions using local techniques for boundary value problems (Ascher, Mattheij & Russell 1995). Local techniques were chosen for their high accuracy. The lower order modes required to satisfy the second order solvability condition were used to compute $R_2$ by numerical integration. At second order, the vertical modes associated with $(\Phi_{lm}, \Phi_{mp}, \Phi_{lp})$ triads for each flow pattern were computed by similar local techniques. The modes for each order were then combined to form the corresponding multidimensional solutions.

## 4. Impermeable mush-liquid interface results and discussion

### 4.1. *Thin mushy layer*

We now focus on a regime in which the mushy layer is thin, similar to the one considered by Amberg & Homsy (1993) in a thin layer approximation. For two-dimensional convection in the form of horizontal rolls, parameter values were chosen to correspond to the two-dimensional results of Amberg and Homsy. An exact comparison is not possible because Amberg and Homsy's model requires the explicit specification of a mushy layer thickness instead of the far-field temperature. In the present model the far-field temperature is specified, and the mushy layer depth is computed as part of the problem. However, to emulate the regime of the thin layer approximation, we choose $\theta_\infty = 3$. Another requirement of the Amberg & Homsy (1993) analysis is that $\mathscr{C} \gg 1$, so we set $\mathscr{C} = 5$. The Stefan number $\mathscr{S}$ is set to 1. This choice of parameters yields a mushy layer thickness of $\delta = 0.281$, which is similar to the choice of $\delta = 0.3$ used by Amberg and Homsy.

Two explicit cases are examined. The first occurs when the variation of permeability with liquid fraction is negligible. In this case, the linear stability analysis yields a critical marginal state with a Rayleigh number of $R_0 = 120.35$ with wavenumber $\alpha = 11.183$. The second case corresponds to a reactive mushy layer and is based on the permeability relation suggested by Worster (1992). In the reactive case, the critical linear Rayleigh number and wavenumber are $R_0 = 157.89$ and $\alpha = 11.217$, respectively. These values are similar to those obtained by Amberg and Homsy.

The maximum vertical velocity occurs at the vertical midpoint in the mushy layer, which is near $z = 0.14$ for the parameter set specified. When the dependence of permeability on liquid fraction is negligible, then $J = 0$. In this case, $R_2 = 16773$. Since $R_2$ is greater than zero, the bifurcation is supercritical. The finite-amplitude solutions $\hat{w}$,$\hat{\chi}$ and $\hat{\theta}$ at the vertical midpoint are calculated as functions of the horizontal coordinate $x$ for both passive mushy layer (constant permeability) and reactive mushy layer (variable permeability) cases. The solutions were evaluated for an amplitude $\epsilon = 0.064$, which is the largest value that makes the liquid fraction not exceed one. A liquid fraction greater than one is unphysical.

For the passive mushy layer case, the results indicate high values of liquid fraction in the neighborhood of the middle and at the endpoints of each cell. These regions of high porosity correspond to regions of rising fluid as are indicated from positive data values for the vertical velocity. The data for the temperature perturbation show that temperature is depressed in the porous region. Recalling that temperature throughout the mush is coupled to solute via the liquidus relation, the colder fluid contains less solute. However, upflow and downflow are symmetric and there is no localization of the solution. For the reactive mushy layer case, the results indicate that localization is present with focused

upflow at the middle and end points of each cell and smaller, more diffuse downflow around at locations half between middle and end points. Such result is suggestive of the formation of chimneys in the focused upflow regions, with slower downward motion where fluid is percolating through regions with increased dendritic growth and subsequent lower permeability. Our generated data in $(x, z)$-plane of the liquid fraction of a single roll parallel to the $y$-axis, suggest that in the region centered at the middle of the cell, there is a chimney extending from bottom to top of the mushy layer surrounded by larger, more solid regions. This result reflects those given for solid fraction in Amberg & Homsy (1993) and the experiments of Chen & Chen (1991).

We now consider the coupling between mush permeability and porosity generated in flow. This coupling accounts for the following physical effect: given that temperature equilibrates much faster than composition, the cold, dilute fluid with incorporate solid via melting and dissolution to equilibrate composition locally. The effect is enabled the model by setting $J = 3$ in the permeability function to reflect a physical permeabilityporosity relationship. In the reactive mushy layer, $R_2 = -214235$ and the bifurcation is subcritical. This transition from supercritical to subcritical with the increase in $J$ is consistent with criterion set forth in Amberg & Homsy (1993).

The principal difference between these results and those found by Amberg & Homsy (1993) are the quantitative values of the Rayleigh number. Here, the values of $R_2$ are larger, but this is due to differences in scaling which do not effect the qualitative nature of the solutions. Specifically, the linear adjoint solutions used here are scaled differently. These results are entirely consistent with the model of Amberg and Homsy. We now extend our results to regimes not accessible in their model.

### 4.2. *Extended parameter study*

The analysis of Amberg & Homsy (1993) was limited in that it presupposed $\theta_\infty \gg 1$ and $\mathscr{C} \gg 1$. For this reason, they were unable study the variation of $\alpha$ and $R$ with the controlling thermodynamic parameters of the mush $\theta_\infty$, $\mathscr{C}$ and $\mathscr{S}$. The current model has no such limitations, so we now examine these variations for passive and reactive mushy layers.

#### 4.2.1. *Linear system variation with far-field temperature*

First, the variation of stability behavior with respect to the supposed far-field temperature $\theta_\infty$ is discussed. The parameters $\mathscr{C}$ and $\mathscr{S}$ kept constant and set to one. From the basic solution, the mushy layer depth $\delta$ is plotted as a function of $\theta_\infty$ in 3. As noted in Worster (1992), the mushy layer thickness is reduced as far-field temperature is increased. The critical Rayleigh number and wavenumber obtained from the linear analysis are shown for the passive case $J = 0$ and the reactive case $J = 3$, shown in figure 4. In both cases $R_0$ and $\alpha$ increase with far-field temperature. The increasing critical Rayleigh number indicates that the mushy layer is more stable, and the increasing wavenumber reflects the fact that instability manifests a shorter length scales. This behaviour is expected in as the mushy layers considered get thinner. As was suggested in the linear results for the thin mush, the reactive mushy layer is generally more stable than the passive case.

#### 4.2.2. *Nonlinear properties*

Due to degeneracy of the linear system, the linear results are applicable to both two- and three- dimensional convection cases. Important quantities due to the nonlinear effects are the coefficients $R_1$ and $R_2$, which are computed in the present study. These coefficients represent leading contributions to the change in $R$ required to obtain finite amplitude $\epsilon$

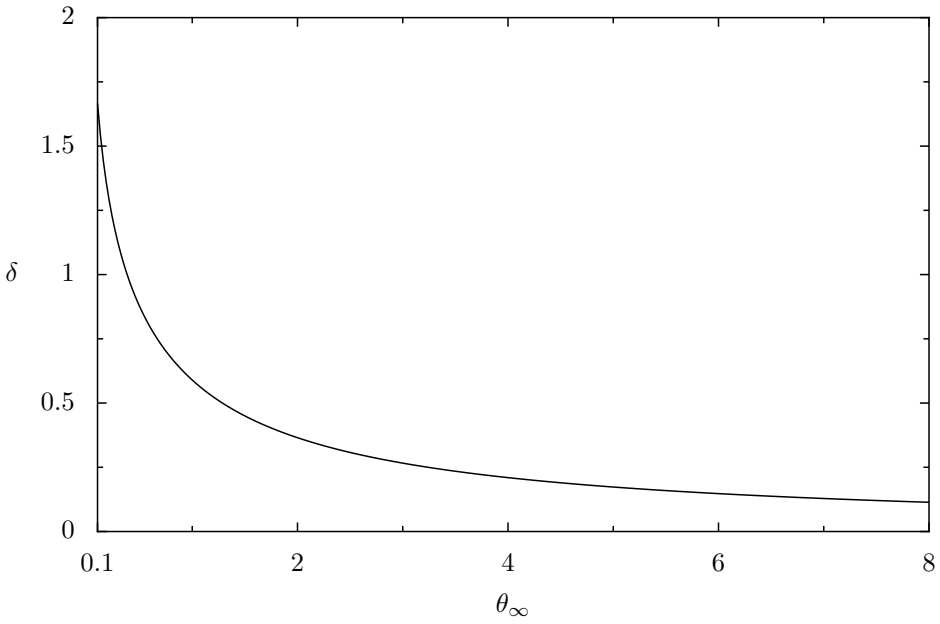


FIGURE 3. Variation of mushy layer depth with the parameter $\theta_\infty$ while $\mathscr{C} = 1$ and $\mathscr{S} = 1$.

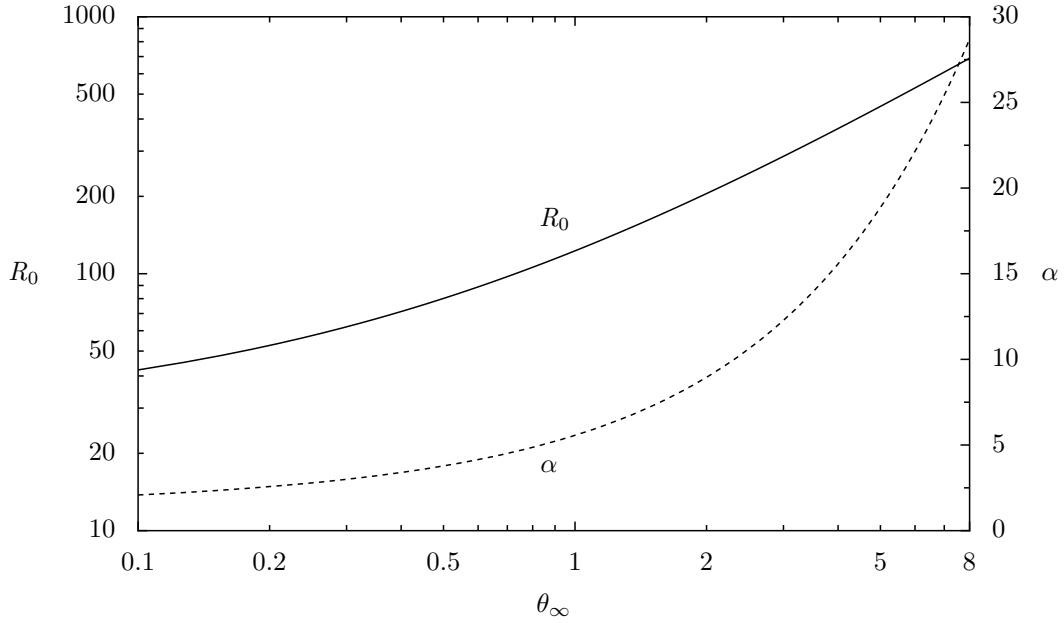


FIGURE 4. Variation of critical Rayleigh number $R_0$ and wavenumber $\alpha$ with the parameter $\theta_\infty$ while $\mathscr{C} = 1$ and $\mathscr{S} = 1$ in a reactive mushy layer with no outflow at the top boundary.

for a nonlinear solution. In terms of these coefficients, the amplitude of convection is of order

$$|\epsilon| = \left\{ \pm |R_1| \pm \left[ R_1^2 + 4R_2(R - R_0) \right]^{1/2} \right\} / (2R_2) \tag{4.1}$$

As can be seen from (4.1), there are four expressions for $|\epsilon|$ corresponding to plus and minus signs in front of the $|R_1|$ term. For the case $\epsilon R_1 < 0$, the two roots with a plus sign

in front of $|R_1|$ provide the expressions for $|\epsilon|$, while the two roots with a negative sign preceeding $|R_1|$ provide the expressions for $|\epsilon|$ if $\epsilon R_1 > 0$. For either case $\epsilon R_1 < 0$ or case $\epsilon R_1 > 0$, the expression with a plus sign in front of the square-root term corresponds to the case where $R_2$ is positive, while the expression with negative sign in front of the square-root term corresponds to the case where $R_2$ is negative.

The expression (4.1) provides some qualitative results about variations of $|\epsilon|$ with respect to $R$. We assume that initially $|\epsilon|$ is sufficiently small. For $\epsilon R_1 < 0$ and $R_2 > 0$, $|\epsilon|$ increases first with decreasing $R$ and then increases with $R$ beyond some value. For $\epsilon R_1 < 0$ and $R_2 < 0$, $|\epsilon|$ increases indefinitely with decreasing $R$, while for $\epsilon R_1 > 0$ and $R_2 > 0$, $|\epsilon|$ increases indefinitely with increasing $R$. For $\epsilon R_1 > 0$ and $R_2 < 0$, $|\epsilon|$ increases first with $R$ and then decreases with increasing $R$ beyond some value. The preferred convection pattern is the one that corresponds to the lowest value of $R$, a definition that often corresponds to observations and agrees with the experimental expectation that the heat or solute transported by the convection pattern (proportional to $\epsilon^2$) should increase with $R$. Further, Iooss & Joseph (1990) have shown that those bifurcation branches for which the amplitude decreases with increasing $R$ are probably unstable and, thus, not physically realizable. These results may be useful to indicate the realization of a particular flow pattern if certain information about the values of $R_1$ and $R_2$ is available.

For the case when $R_1 = 0$, which can correspond to two-dimensional rolls, rectangles, and square pattern convection, then the sign of $R_2$ determines whether the steady solution exists for values of $R$ above or below $R_0$. When $R_1 = 0$ and convection is supercritical, where $R > R_0$, the amplitude of convection increases with $R$ and is largest provided the value of $R_2$ is smallest among all the solutions to the nonlinear problem. For $R_1 = 0$ and subcritical convection, where $R < R_0$, the amplitude of convection decreases with increasing $R$ and is largest, provided $|R_2|$ is the minimum among all solutions. Variations of $R_1$ with respect to different parameters provide information about various destabilizing and stabilizing features for hexagonal convection. However, the information about $R_2$ for hexagons as well as non-hexagons is useful in calculating solute flux, and in cases where $R_1$ is negligible or zero.

In the present problem, the coefficients $R_1$ and $R_2$ are due to the nonlinear convective terms in the temperature equation and nonlinear interactions between the flow velocity and the non-uniform, nonlinear permeability associated with the perturbation to the basic state liquid fraction.

It should also be noted that the variations of $R_1$ with respect to different parameters provide information about various destabilizing and stabilizing features for the hexagonal convection. However, the information about $R_2$ for hexagons and nonhexagons is useful in the sense that since $R_2$ is the second-order coefficient in the expansion for R in powers of , $R_2$ plays useful roles in calculating the solute flux and the order of magnitude of in (4.1) and in cases where $R_1$ is zero or becomes negligible.

4.2.3. *Nonlinear system variation with far-field temperature*

We now consider patterns of convection from nonlinear terms, and as in the linear system analog, $\mathscr{S}$ and $\mathscr{C}$ are kept constant and set to one. The simplest regular solution is two-dimensional rolls. For this pattern, it was found that $R_1$ is zero. First, the second order correction to the Rayleigh number $R_2$ is calculated versus $\theta_\infty$ in the case $J = 0$ and in the case $J = 3$ (figure 5), where $R_2$ for rolls is designated by $R_2$ . In both cases $R_2 < 0$ for all the considered values of indicating subcritical bifurcation. In these cases bifurcation is probably always subcritical. $R_1$ was also found to be zero for squares and rectangles. Next, we calculated $R_2$ for squares and rectangles in both cases of passive mush ($J = 0$) and reactive mush ($J = 3$). In the passive mush case, $R_2$ for squares,

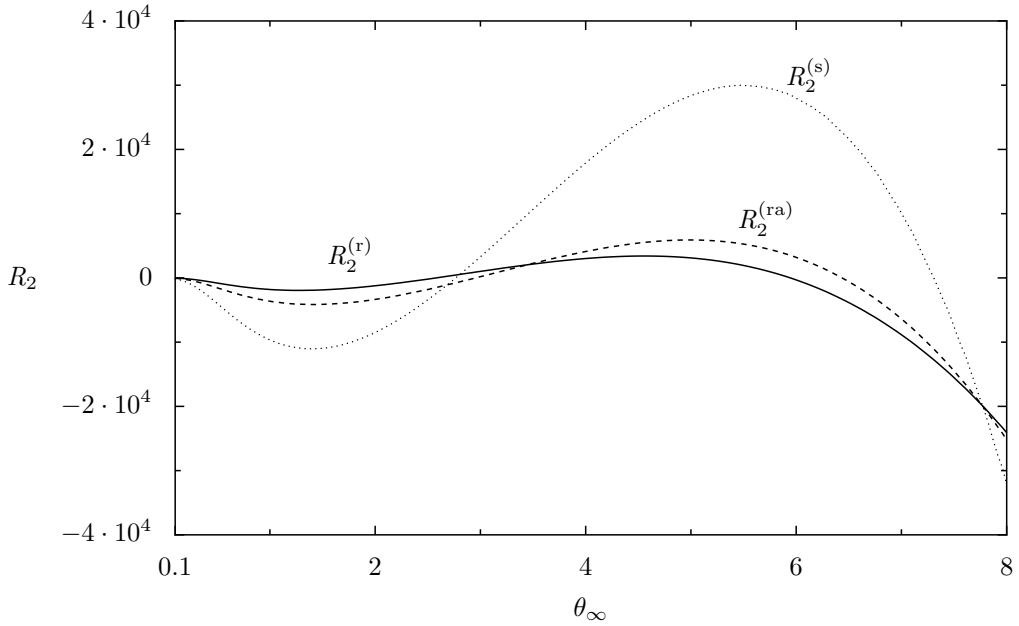


FIGURE 5. Variation of $R_2$ with the parameter $\theta_\infty$ while $\mathscr{C} = 1$ and $\mathscr{S} = 1$ in a reactive mushy layer with no outflow at the top boundary.

designated by $R_2^{(s)}$ , and $R_2$ for rectangles, designated by $R_2^{(ra)}$, are found to be negative and $|R_2^{(s)}| > |R_2^{(ra)}| > |R_2^{(r)}|$ throughout the considered values of the far-field temperature.

However, in the reactive mush case (figure 5), there is an intermediate range in $\theta_\infty$ where $|R_2^s|$ and $|R_2^{ra}|$ (for $\gamma = 45°$) are positive, indicating supercritical bifurcations for these patterns in such intermediate range of far-field temperature.

4.2.4. *Nonlinear system variation with concentration ratio*

We now considered effects of variation of $\mathscr{C}$, where both $\mathscr{S}$ and are kept constant and set to one. Physically, the concentration ratio $\mathscr{C}$ may b viewed as the nondimensional composition of the consituent dendrites formed during solidification. Out calculated result for the mushy layer depth indicates that increases monotonically with $\mathscr{C}$. A larger concentration ratio also increases porosity. Our generated data for $R_0$ and versus $\mathscr{C}$ show that $R_0$ increases slightly and decreases strongly with $\mathscr{C}$ in the passive mush case, while both of these quantities decrease strongly with increasing $\mathscr{C}$ in the reactive mush case. Since the increase in porosity is not coupled with the permeability in the passive mush case, the resulting effect on the stability of the mush is not large. The mush becomes slightly more stable in this case. In contrast, the more physical case of the reactive mush has coupled porosity and permeability, such that permeability increases cubically with porosity and $\mathscr{C}$ can be destabilizing in this case. In both the reactive and passive mushy layer cases, linear stability analysis yields increasing wavelength with increasing $\mathscr{C}$, consistent with the larger mushy layer.

The generated data for $R_2$ versus $\mathscr{C}$ in the cases of rolls, rectangles and squares indicate that $R_2$ is negative for the passive mush implying subcritical bifurcation for such patterns. However, the corresponding results for the reactive mush (figure 9) indicate supercritical bifurcations for each of such patterns, provided $\mathscr{C}$ is sufficiently small. The generated data for $R_1$ versus $\mathscr{C}$ in the case of hexagons for the passive and mush indicate that $R_1 < 0$, while $R_1 > 0$ for the reactive mush only for sufficiently small $\mathscr{C}$. Our generated

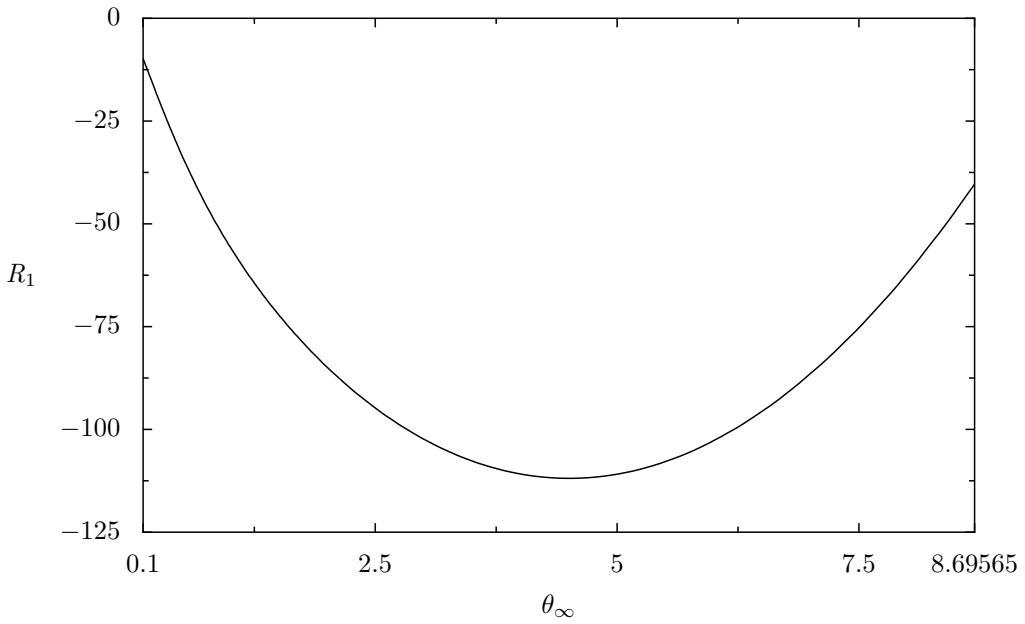


FIGURE 6. Variation of $R_1$ with the parameter $\theta_\infty$ while $\mathscr{C} = 1$ and $\mathscr{S} = 1$ in a passive mushy layer with no outflow at the top boundary.

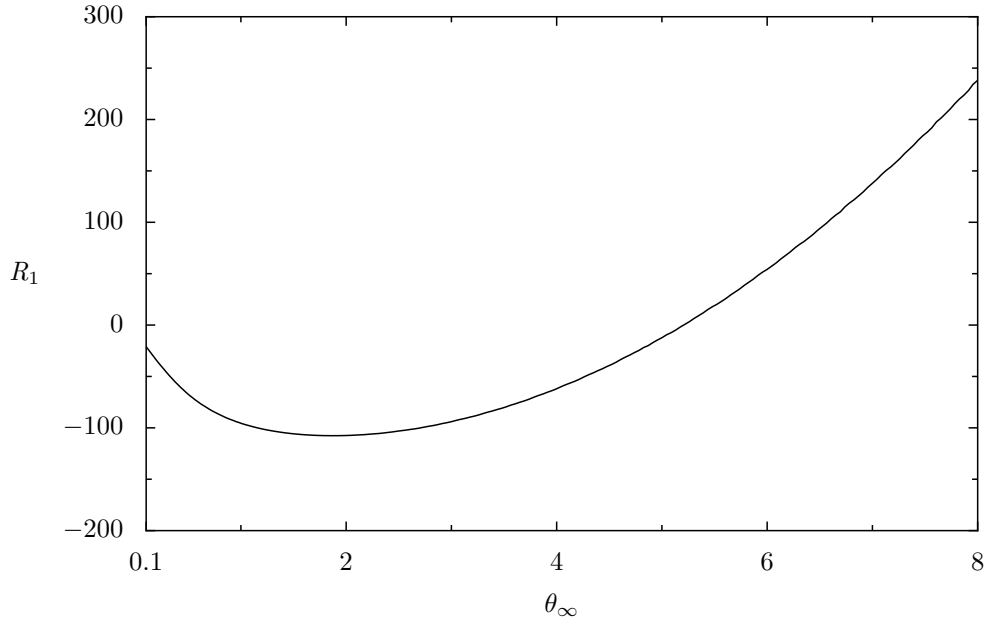


FIGURE 7. Variation of $R_1$ with the parameter $\theta_\infty$ while $\mathscr{C} = 1$ and $\mathscr{S} = 1$ in a reactive mushy layer with no outflow at the top boundary.

data for $R_2$ versus $\mathscr{C}$ for the hexagons indicate that for the passive mush, $R_2$ increase monotonically with $\mathscr{C}$ and $R_2 > 0$,unless $\mathscr{C}$ is too small. The corresponding results for the reactive mush indicate that $R_2 > 0$ only for very small $\mathscr{C}$, and as $\mathscr{C}$ increases from small to large values, $R_2$ decreases rapidly first and then increasing modestly with $\mathscr{C}$.

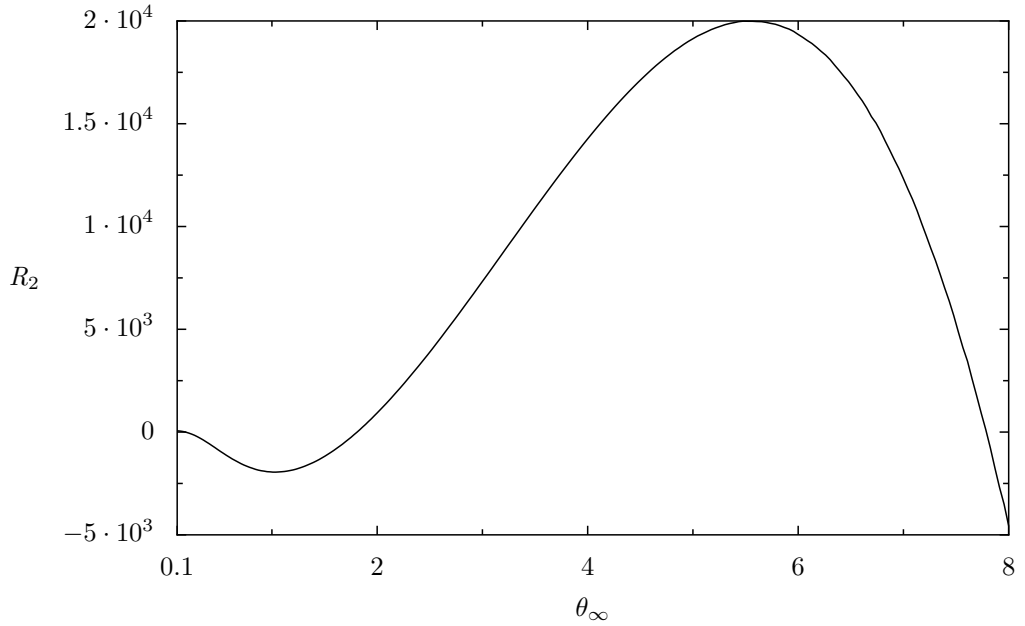


FIGURE 8. Variation of $R_2$ with the parameter $\theta_\infty$ while $\mathscr{C} = 1$ and $\mathscr{S} = 1$ in a reactive mushy layer with no outflow at the top boundary.

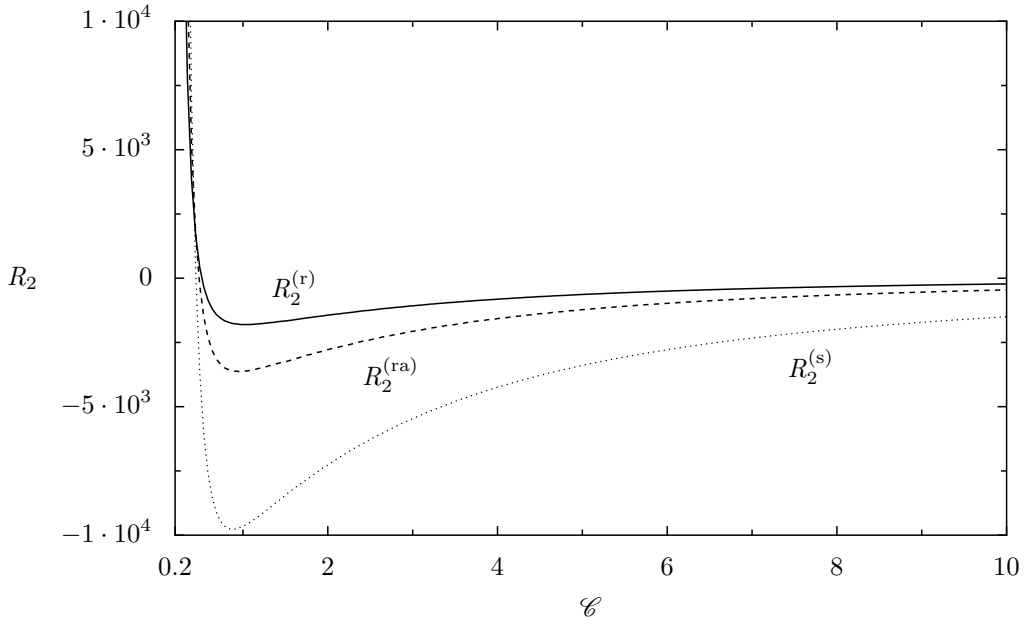


FIGURE 9. Variation of $R_2$ for non-hexagonal patterns with the parameter $\theta_\infty$ while $\mathscr{C} = 1$ and $\mathscr{S} = 1$ in a reactive mushy layer with no outflow at the top boundary.

4.2.5. *Nonlinear system variation with Stefan number*

Our calculated data for varies quantities versus $\mathscr{S}$ with $\mathscr{C}$ and $\theta_\infty$ kept at the constant value of 1 indicate the following results. The mushy layer depth decreases with increasing $\mathscr{S}$. However, in contrast to the effect of the far-field temperature, the effect of increasing

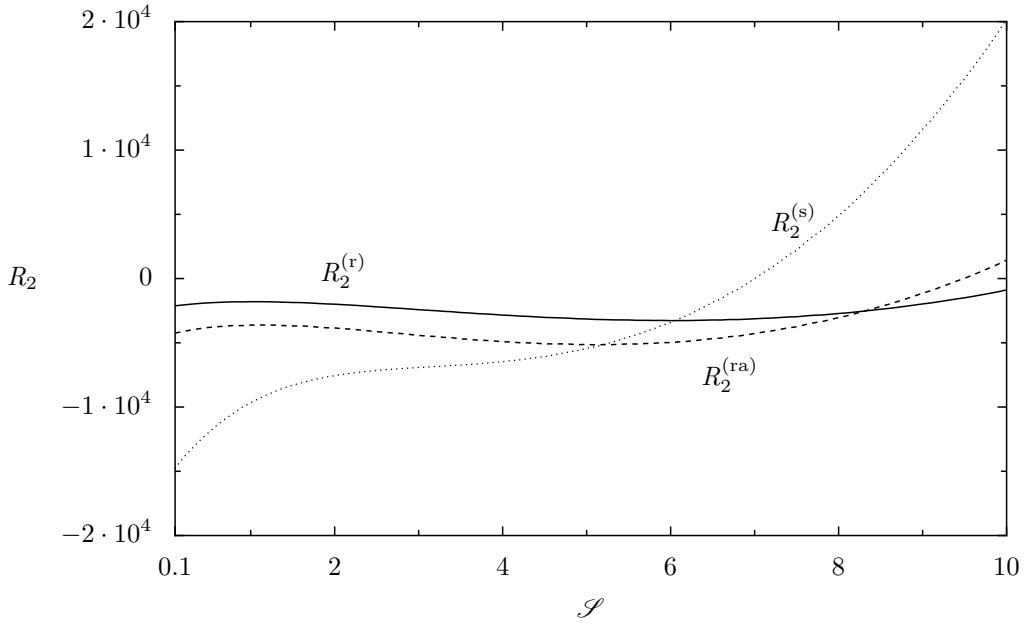


FIGURE 10. Variation of $R_2$ with the parameter $\mathscr{S}$ for non-hexagonal patterns while $\mathscr{C} = 1$ and $\theta_\infty = 1$ in a reactive mushy layer with no outflow at the top boundary.

Stefan number on the linear perturbation is to destabilize the flow. The result is that higher $\mathscr{S}$ results in lower $R_0$ and higher for both $J = 0$ and $J = 3$ cases. Stefan number is representative of latent heat in the system, and a larger latent heat results fewer dissolved dendrites. The fluid is then less dense and more buoyant. $R_2$ for the cases of non-hexagons decreases monotonically with increasing $\mathscr{S}$ and $R_2^{\mathrm{ra}} < R_2^{\mathrm{s}} < R_2^{\mathrm{r}} < 0$ in the passive mush implying subcritical bifurcations for such patterns. The corresponding results for the reactive mush (figure 10) indicate that supercritical bifurcations can be possible for squares and rectangles only for sufficiently large $\mathscr{S}$. $R_1$ for hexagons is negative and decreases monotonically with increasing $\mathscr{S}$ for both passive mush and reactive mush (figure 11) implying that subcritical up-hexagons and supercritical down-hexagons are possible. For the passive mush, $R_2$ for hexagons is positive. For the reactive mush, figure 12 presents variation of $R_2$ for hexagons versus $\mathscr{S}$, which indicates that supercritical hexagons are possible at higher amplitudes.

## 5. Permeable mush-liquid interface results and discussion

### 5.1. *System variation with far-field temperature*

The variation of mushy layer depth in the case of permeable mush-liquid interface is identical to the variation in the impermeable case because the difference in the two models is dynamic coupling and the mushy layer depth is determined for the static mushy layer. As in the impermeable case, $\delta$ decreases with increasing $\theta_\infty$. Here we look at the effect of varying $\theta_\infty$, while holding $\mathscr{C} = 1$ and $\mathscr{S} = 1$. We found that we needed to consider some differences in the $\theta_\infty$ ranges for the passive and reactive cases because of differences in numerical accessibility of values of $\theta_\infty$ for the two cases.

The linear analysis of variation of $R_0$ and $\alpha$ with respect to $\theta_\infty$ indicates that, as in the case of the impermeable interface, both $R_0$ and $\alpha$ increase with far-field temperature for both passive and reactive mush cases. For the passive mush, variation of the Rayleigh

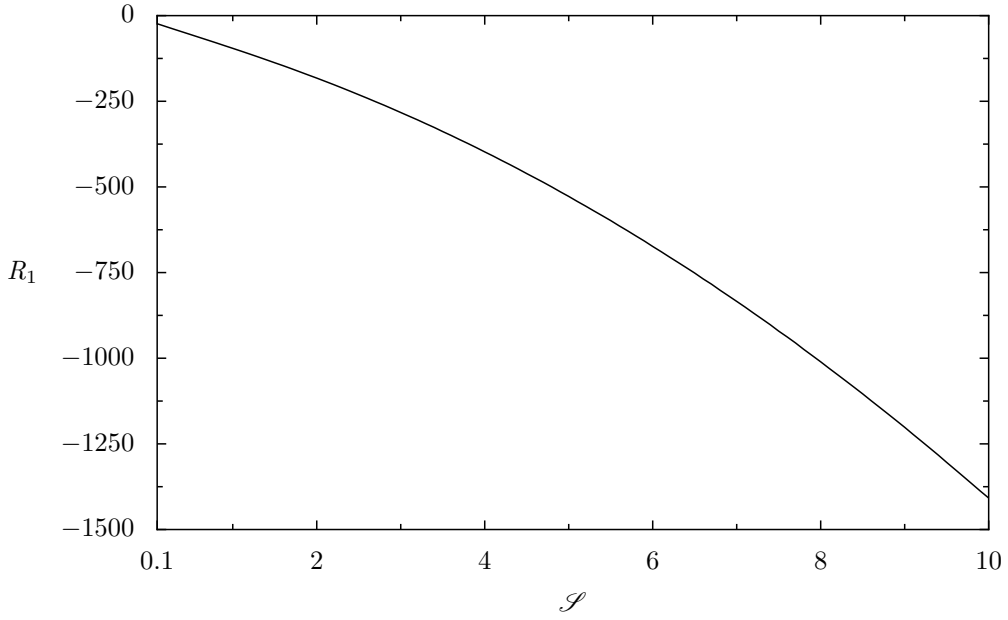


FIGURE 11. Variation of $R_1$ with the parameter $\mathscr{S}$ for hexagons while $\mathscr{C} = 1$ and $\theta_\infty = 1$ in a reactive mushy layer with no outflow at the top boundary.

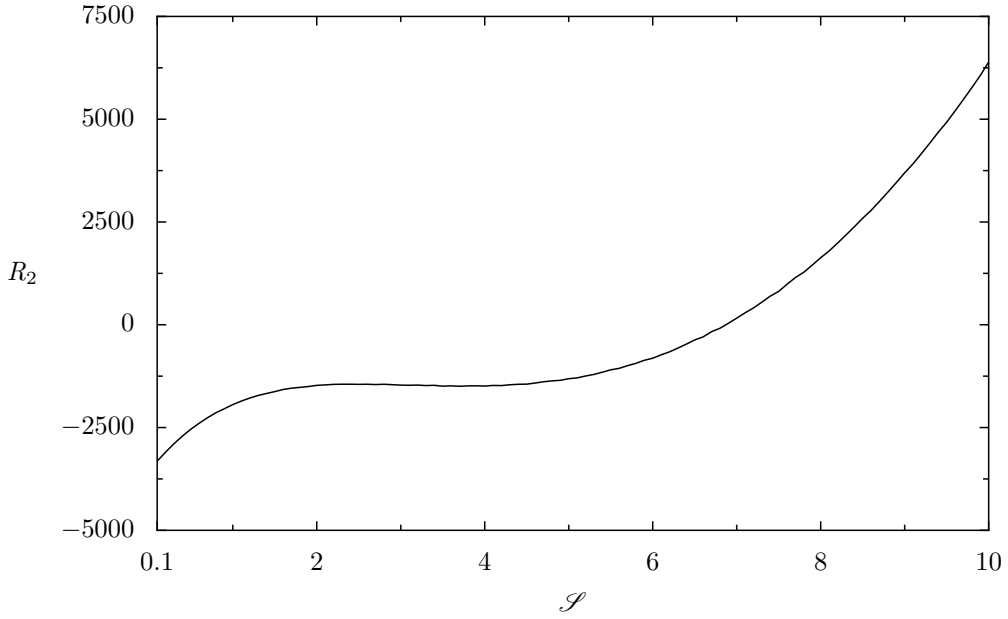


FIGURE 12. Variation of $R_2$ with the parameter $\mathscr{S}$ for hexagons while $\mathscr{C} = 1$ and $\theta_\infty = 1$ in a reactive mushy layer with no outflow at the top boundary.

number and wavenumber with the far-field temperature varying from 0.3 to 5 were studied. At $\theta_\infty = 0.3$, the Rayleigh number is 18.7947. As far-field temperature is increased to 5, $R_0$ increases to 105.977. The minimum wavenumber is 2.1831, which corresponds to a mushy layer depth of 1.1146, and the maximum wavenumber 13.5374 occurs with a depth of 0.1732. From the linear stability in the reactive case $J = 3$, studied for the range

$\theta_\infty = 0.1$ to 4, the Rayleigh number varies from $R_0 = 34.9664$ to 271.36. The Rayleigh number is generally larger and increases more rapidly the the non-reacting case. When $\theta_\infty = 0.3$, $R_0$ is 48.7509 as opposed to 18.7947 in the passive case. At $\theta_\infty = 0.1$, the critical wave number is 1.7535. It increases to 13.3004 as the far-field temperature is increased to 4. The difference in wavenumbers between $J = 0$ and $J = 3$ cases is smaller.

We now consider the formation of two- and three-dimensional flow patterns near the onset of convection. First, three non-hexagonal patterns are considered: two-dimensional rolls, three-dimensional rectangular cells with $\gamma = 45^\circ$ and square cells. For the inert mush, $|R_2|$ increases with $\theta_\infty$ for rolls and rectangles, and $R_2^{(\mathrm{ra})} < R_2^{(\mathrm{s})} < R_2^{(\mathrm{r})}$ in the range $[0.3, 5]$ studied for $\theta_\infty$. The maximum $R_2^{(\mathrm{r})}$ is $-42.6541$ at$\theta_\infty = 0.3$ and the minimum is $-255.442$ at $\theta_\infty = 5$. For rectangles, $R_2^{(\mathrm{ra})}$ decreases with increasing $\theta_\infty$ from 70.6546 to 385.264. The range of Rayleigh number corrections for squares falls between the curves for rolls and rectangles, decreasing from 31.7683 at $\theta_\infty = 0.3$ to 377.872 at $\theta_\infty = 5$. Extrapolating the curves for rolls and rectangles suggests that these patterns may become supercritical for smaller $\theta_\infty$. The Rayleigh number correction for squares, where there is a larger angle $\gamma$ ($\gamma = 90$), increases slightly with $\theta_\infty$ for $\theta_\infty < 0.4$ but decreases as $\theta_\infty$ is increased more. Thus all the three patterns show an increasing tendency toward subcritical branches as far-field temperature is increased.

In figure 13, the result on second order Rayleigh number correction of varying far-field temperature from 0.1 to 4 for the reactive much with $J = 3$ is shown. The magnitudes of $R_2$ are an order larger than the passive case, however it is the qualitative behavior that is of interest. In the reactive case, the variation in $R_2$ as $\theta_\infty$ is increased become more extreme as angle $\gamma$ increases. The curves are no longer strictly decreasing over the range of considered. However, as in the passive case, subcritical rolls may be possible over the whole range of the far-field temperature considered. However, in the case of squares, the results show that $\mathscr{R}_\mathrm{m}$ may be supercritical between $\theta_\infty = 2.3699$ and 2.9623. Comparing the results shown in figure 13 to the corresponding ones for the impermeable interface case (figure 5), we find qualitative similarities in relation to the relative behavior and variations of $R_2$ for these patterns, but quantitative values and variations are different.

For hexagonal cells, the first order correction $R_1$ is plotted versus far-field temperature in figure 14 for the passive mush and in figure 15 for the reactive mush. The shapes of the $R_1$curves in the passive and reactive cases are similar. Both curves indicate decreasing $R_1$ with increasing when is small, but then turning to increase at higher temperatures. In both cases $R_1$ changes sign as far-field temperature is increased further. In the passive case, $R_1$ changes sign at $\theta_\infty = 4.624$. In the reactive case, $R_1$ changes sign at a lower temperature $\theta_\infty = 2.737$. Comparing these results to the corresponding ones shown in the figures 6 and 7 for the impermeable interface case, we find similar shapes, but in the permeable interface case $R_1$ becomes positive at lower values of the far-field temperature in both passive and reactive cases. This result indicates, in particular, that in the permeable case, there is more inclination toward subcritical down-hexagons.

The second order correction to the Rayleigh number $R_2$ for hexagons in the passive case is calculated versus far-field temperature in the domain $[0.3, 5]$. Over this domain $R_2 < 0$, and this tendency towards subcritical hexagons being unstable and increases with $\theta_\infty$. However, the result for the reactive much (figure 16) is different. As suggested by the trend of increasing $\theta_\infty$ in the non-hexagonal case, in the hexagonal case, which has larger angle $\gamma$ ($\gamma = 60^\circ$), there is a region where $R_2$ is positive. In contrast to the non-hexagonal case, $R_2 > 0$ in the range $\theta_\infty = 1.7946$ to 3.2754, which indicates the possibility of realizable subcritical hexagons since according to our earlier discussion of

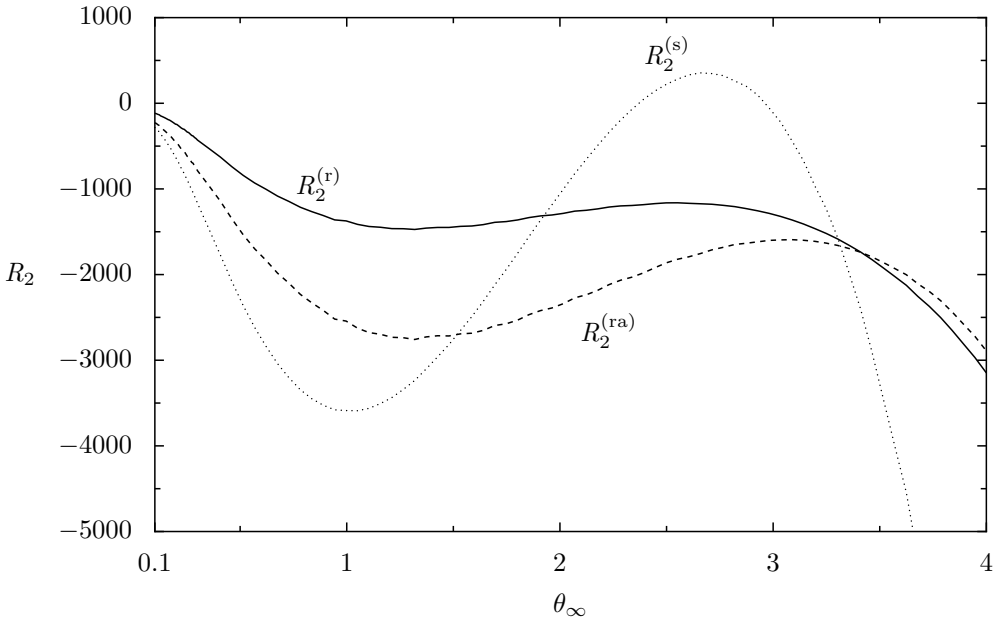


FIGURE 13. Variation of $R_2$ with the parameter $\theta_\infty$ for non-hexagonal patterns while $\mathscr{C} = 1$ and $\mathscr{S} = 1$ in a reactive mushy layer with outflow at the top boundary.

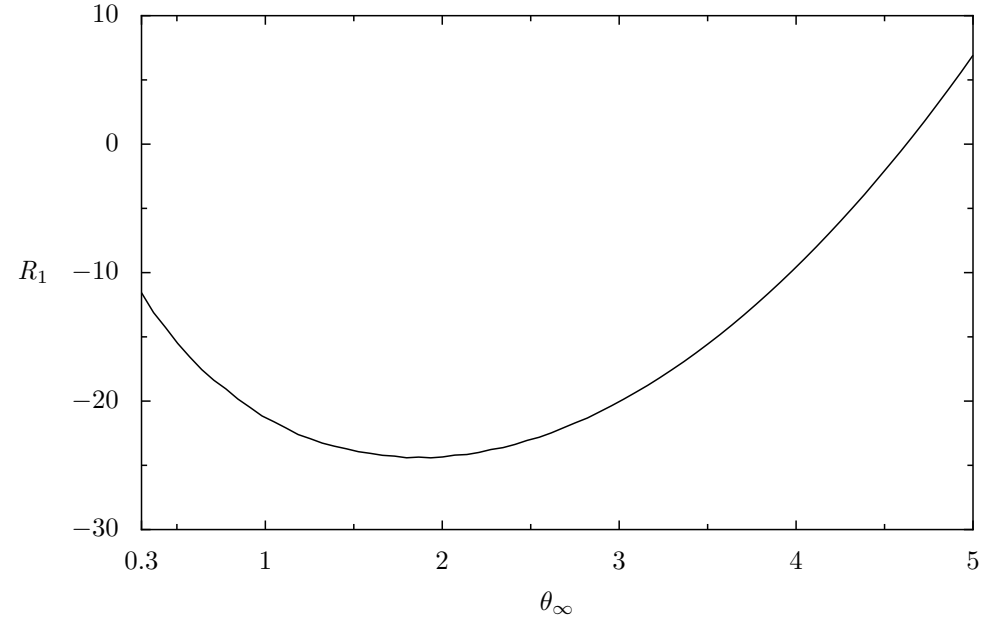


FIGURE 14. Variation of $R_1$ with the parameter $\theta_\infty$ for non-hexagonal patterns while $\mathscr{C} = 1$ and $\mathscr{S} = 1$ in a passive mushy layer with outflow at the top boundary.

(4.1), it could correspond to the smallest value of $\mathscr{R}_\mathrm{m}$ and contains a regime where $|\epsilon|$ increases with $\mathscr{R}_\mathrm{m}$.

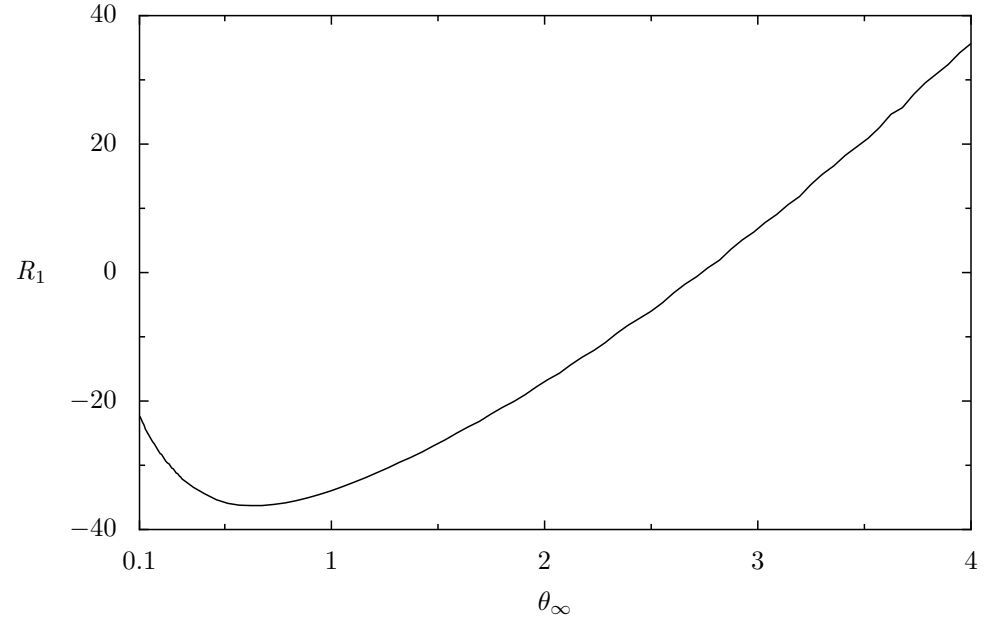


FIGURE 15. Variation of $R_1$ with the parameter $\theta_\infty$ for non-hexagonal patterns while $\mathscr{C} = 1$ and $\mathscr{S} = 1$ in a reactive mushy layer with outflow at the top boundary.

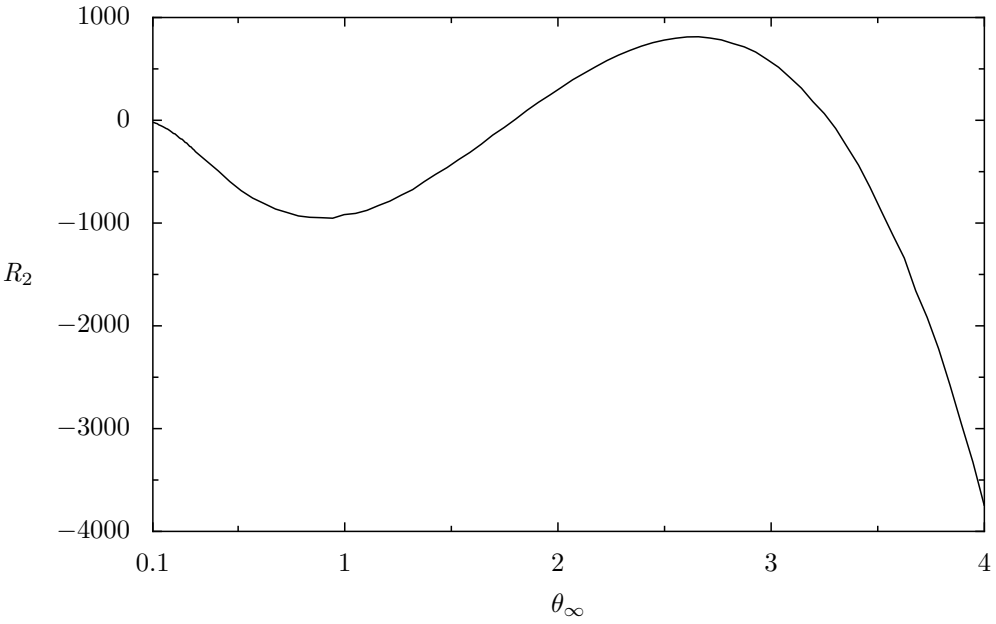


FIGURE 16. Variation of $R_2$ with the parameter $\theta_\infty$ for non-hexagonal patterns while $\mathscr{C} = 1$ and $\mathscr{S} = 1$ in a reactive mushy layer with outflow at the top boundary.

### 5.2. *System Variation with Concentration Ratio*

We studied the effect of varying $\mathscr{C}$ by setting the $\theta_\infty$ and $\mathscr{S}$ to one. First, we generated data for $R_0$ and $\alpha$ versus $\mathscr{C}$ for the non-reactive case. A range of $\mathscr{C} = 0.5$ to 13 is considered. The critical Rayleigh number does not vary dramatically over this range. At

$\mathscr{C} = 0.5$, $R_0 = 30.6758$, whereas at $\mathscr{C} = 13$, $R_0 = 40.0419$. This increase in stability differs from the result of Worster (1992) for a reactive mushy layer with a superposed liquid. One explanation may be due to the following effect. In the passive case, permeability is constant and decoupled from porosity. As we consider larger and larger concentration ratios, pemeability as well as Stefan number are fixed. During a phase change in the vicinity of a dendrite latent heat represented in the Stefan number is quickly diffused over the larger mushy layer. Without the competing effect of increased permeability, this effect is mildly stabilizing.

In contrast, the reactive mushy layer critical Rayleigh number becomes less stable over the same range of $\mathscr{C}$. Here $R_0$ drops from $R_0 = 174.83$ for $\mathscr{C} = 0.5$ to $R_0 = 44.491$ for $\mathscr{C} = 13$. This trend agrees with the result reported in Worster (1992) for a reactive mushy layer with $J = 3$. In the reactive case, the increase in porosity results in a strong increase in permeability, allowing greater fluid mobility with less dissipation for a given perturbation.

In both the $J = 0$ and $J = 3$ cases, critical wavenumber decreases with $\mathscr{C}$ The wavenumber is 4.3061 in the inert case and 5.7619 in the reactive case at $\mathscr{C} = 0.5$. At the other end of the considered range, $\mathscr{C} = 13$, the wavenumber is 3.4757 in the inert case verses 3.5348 in the reactive case. This decrease is small compared with the amount of variation with the other parameters.

Next we consider the trends for the formation of non-hexagonal patterns when $\mathscr{C}$ is varied. In the passive mushy layer, the Rayleigh number correction $R_2$ is less than zero over the entire range of $\mathscr{C}$ considered for two-dimensional rolls and three-dimensional rectangles and squares. This tendency toward possible subcritical patterns is increasing from $\mathscr{C} = 0.5$ to $\mathscr{C} = 2.8551$ for rolls, 2.6739 for rectangles and 1.4058 for squares. As $\mathscr{C}$ is increased further for each pattern, the tendency toward subcriticality decreases. If we extrapolate the results to values of $\mathscr{C}$ smaller than those shown in the figures, the results show a possible tendency toward supercriticality for $\mathscr{C} < 0.5$.

In the reactive mush (figure 17), $R_2$ for squares is positive for $\mathscr{C} = 0.5$, while the other two patterns are subcritical, as in the inert case. As shown in figure 17, all three patterns have a similar trend of decreasing $R_2$ from $\mathscr{C} = 0.5$ to $\mathscr{C} = 1.2246$ for rectangles and squares and 1.4058 for rolls. For larger concentration ratios, $R_2$, while negative throughout the remaining range of $\mathscr{C}$, increases.

We calculated the values of $R_1$ for hexagons in the interval $[0.5, 13]$ for $\mathscr{C}$ for both passive and reactive mush cases. For the passive and reactive (figure 18) cases, $R_1 < 0$ over entire and most of the domain of $\mathscr{C}$ considered. In the reactive case, as shown in the figure 18, $R_1$ becomes positive for very small $\mathscr{C}$ indicating possible subcritical downhexagons or supercritical up-hexagons for such small values of $\mathscr{C}$. Comparing these results to the corresponding ones in the impermeable interface case, we find qualitatively similar behavior.

The generated data for the second order Rayleigh number correction for hexagons and in the case of passive mush indicate that supercritical hexagons may be possible for $\mathscr{C} > 1.6027$. As in the linear stability results, the tendency for $R_2$ in the reactive case is reversed from the passive case. In the reactive case, the results indicate that supercritical hexagons are not possible for $\mathscr{C} > 0.6429$. $R_2$ decreases from $\mathscr{C} = 0.5$ to 1.5870 in the reactive case but then tends to increase as concentration ratio is increased further.

### 5.3. *System Variation with Stefan Number*

We now hold the far-field temperature and concentration ratio fixed at one and vary the Stefan number. Increasing Stefan number under these conditions decreases the size of the mushy layer. A Stefan number range of 0.1 to 10 is considered. The critical wavenumber

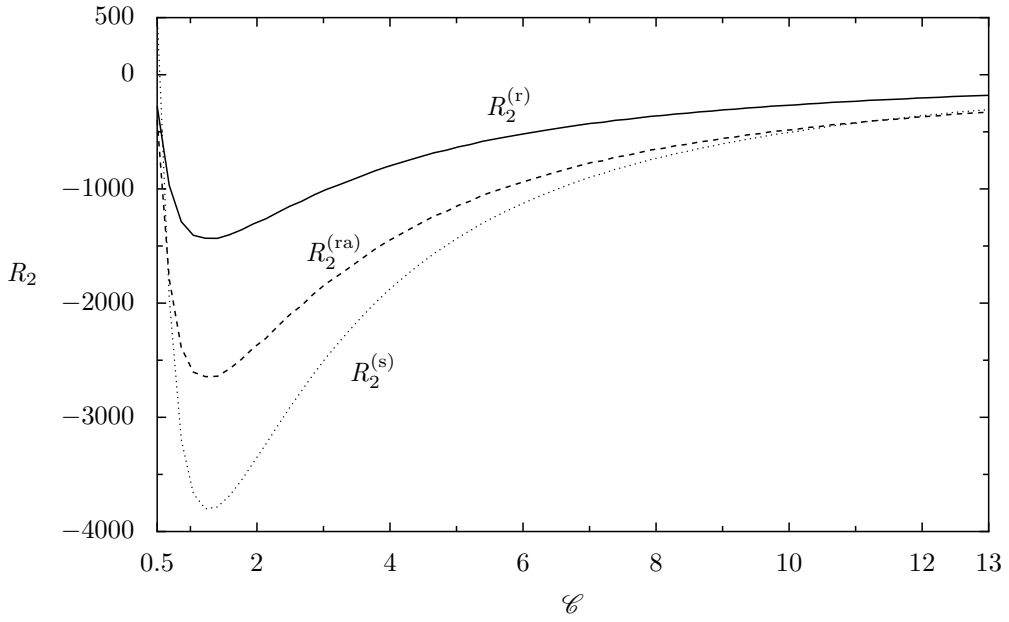


FIGURE 17. Variation of $R_2$ with the parameter $\mathscr{C}$ for non-hexagonal patterns while $\theta_\infty = 1$ and $\mathscr{S} = 1$ in a reactive mushy layer with outflow at the top boundary.

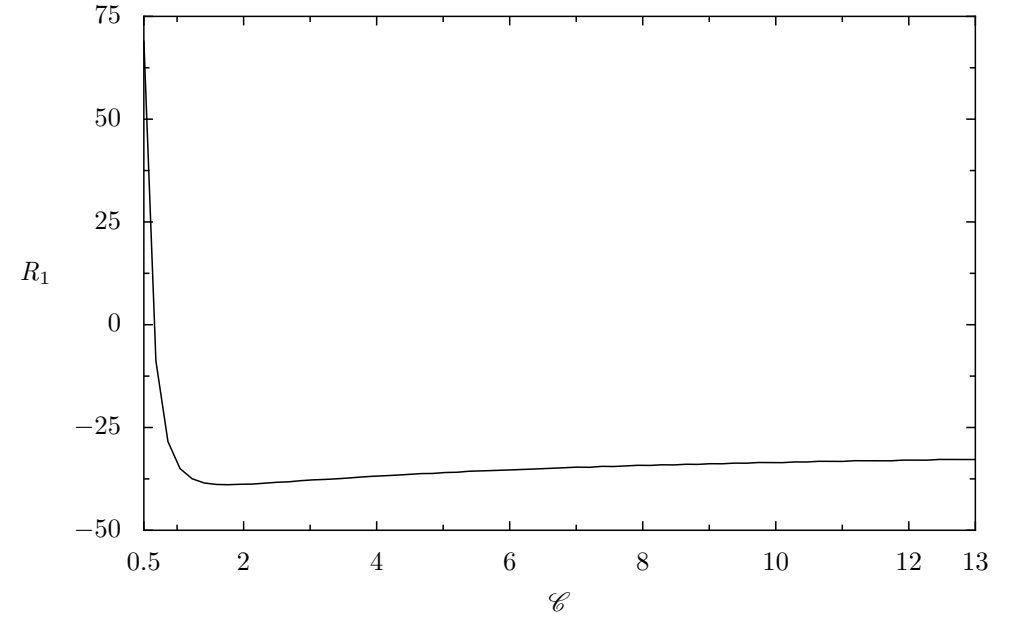


FIGURE 18. Variation of $R_1$ with the parameter $\mathscr{C}$ for hexagons while $\theta_\infty = 1$ and $\mathscr{S} = 1$ in a reactive mushy layer with outflow at the top boundary.

increases from $\alpha = 3.4615$ to 8.8461 over the the range of $\mathscr{S}$ considered in the non-reactive mush case. Variation of wavenumber in the reactive case is slightly larger in the non-reactive case but otherwise the variation is similar between the two cases. For $\mathscr{S} = 0.1$, $\alpha = 4.0769$ and at $\mathscr{S} = 10$, $\alpha = 10.326$.

For the passive mushy layer, the critical Rayleigh number decreases from 40.5453 for

$\mathscr{S} = 0.1$ to 17.0932 at $\mathscr{S} = 10$. When far-field temperature was increased, it was found that the size of the mushy layer decreased and there was stabilization of the system. In contrast, increasing the Stefan number also decreases the size of the mushy layer but the system is less stable. For the reactive mush case, $R_0$ has the same basic trend. $R_0 = 119.478$ at $\mathscr{S} = 0.1$ and $R_0$ decreases to 43.807 at $\mathscr{S} = 10$. The change is larger than for the inert case, but the reactive case remains a generally more stable system.

Our generated $R_2$data for the non-hexagonal patterns lead to the results, which are briefly as follows. For the passive mush case, $R_2$ decreases with increasing $\mathscr{S}$ and $R_2^{(\mathrm{ra})} < R_2^{(\mathrm{s})} < R_2^{(\mathrm{r})} < 0$ throughout the range of values considered for $\mathscr{S}$. Hence, tendency toward subcriticality is stronger for rectangles followed by squares and rolls. In contrast, non-hexagonal patterns in $J = 3$ case may be subcritical or supercritical, depending on the value of $\mathscr{S}$. Rolls would be subcritical when $\mathscr{S} < 9.0687$, rectangles when $\mathscr{S} < 7.8707$, and squares when $\mathscr{S} < 5.8165$. For large $\mathscr{S}$ values, $R_2 > 0$, and the tendency toward supercriticality is increased for all these patterns.

For hexagonal convection, the first-order Rayleigh number correction $R_1$ for both passive and reactive mush cases is negative and monotonically decreases with increasing $\mathscr{S}$. Comparing these results to the corresponding ones for the impermeable interface case, we find qualitatively similar behavior, but $R_1$ is consistently smaller in the impermeable case. The variation of the second-order Rayleigh number correction $R_2$ with respect to $\mathscr{S}$ for hexagons is different. For the passive mushy layer, $R_2$ decreases with $\mathscr{S}$, it is positive for $\mathscr{S} < 0.7309$ and negative for $\mathscr{S} > 0.7309$. If $J = 3$, the trend is reversed. $R_2$ is positive for $\mathscr{S} > 5.9672$ and negative otherwise.

## 6. Conclusions and some remarks

We investigated the problem of nonlinear buoyant convection in mushy layers during alloy solidification for both cases of impermeable and permeable mush-liquid interfece. We analyzed the effects of several parameters on two- and three-dimensional steady convection patterns in the mushy layers for both constant and variable permeability. Using both analytical and computational methods, we determined the steady solutions admitted by the weakly nonlinear problem in different ranges of the values of the parameters.

The most important result of the present study was the prediction of subcritical down-hexagonal pattern for the variable permeability case that corresponds to the smallest value of the Rayleigh number. Such pattern was detected to exist more often in the cases of reactive mushy layers, even though other types of convection pattern such as rolls, squares, rectangles and up-hexagons in both subcritical and supercritical regimes, as well as supercritical down-hexagons, were also predicted in particular range of values of the parameters for either passive or reactive mushy layers with impermeable or permeable interfaces.

In regard to different types of flow patterns predicted in this paper, it should be noted that there are a number of natural and engineering systems where each of such patterns may be observed under certain conditions (Hoyle 1998). In the present system, certain conditions or effects that may be responsible for the prediction of particular flow patterns are provided as follows. Prediction of the supercritical rolls depended on the imposed isothermal boundary conditions. Prediction of subcritical or supercritical hexagons depended on the nonlinear basic states, which impose certain asymmetry on the fluid layer, and the variability of the permeability with respect to the liquid fraction. Prediction of supercritical rectangular and square patterns depended on the nonlinear permeability variations associated with perturbations to the basic state liquid fraction.

Prediction of subcritical non-hexagonal patterns depended on the large rate of increase of the permeability with respect to the porosity.

About the significance of the hexagonal or non-hexagonal patterns, let us assume that the magnitude of the amplitude of the observed convection pattern increases with the Rayleigh number and the preferred convection pattern corresponds to the smallest value of the Rayleigh number. Then within the present weakly nonlinear analyses and calculations, we may expect preference of subcritical hexagons for sufficiently small $|\epsilon|$ and preference of supercritical non-hexagons at higher values of $|\epsilon|$, but we may not expect preference of either subcritical non-hexagonal patterns or supercritical hexagons.

Finally, in regard to the stability of the finite-amplitude flow solutions predicted in the present study, it should be noted that present perturbation approach is generally incapable to carry out a standard stability analysis (Busse 1967) due to the fact that the asymmetries in the present problem, which cause non-zero values for $R_1$, are, in general, not small. A stability investigation, which requires extensive work and remains a topic for future study, will require full numerical computation of both finite-amplitude solutions and their stability analysis without any use of the perturbation approach.

## Appendix

The expressions for the $3 \times 3$ matrix operators $\boldsymbol{\mathcal{L}}$ and $\hat{\boldsymbol{\mathcal{L}}}$ and the vector operator $\boldsymbol{\mathcal{N}}$ are given below

$$\boldsymbol{\mathcal{L}} = (\mathcal{L}_1, \mathcal{L}_2, \mathcal{L}_3)^{\mathrm{T}}, \tag{A 1a}$$

where $\mathcal{L}_i$ $(i = 1, 2, 3)$ is the $i$-th row of the matrix $\boldsymbol{\mathcal{L}}$ and given by

$$\mathcal{L}_1 \equiv \left\{ \left(\tfrac{\partial}{\partial t} - \tfrac{\partial}{\partial z} - \triangle\right), \left[\mathscr{S}\left(\tfrac{\partial}{\partial t} - \tfrac{\partial}{\partial z}\right)\right], \left[\left(-\tfrac{d\theta_b}{dz}\right)\triangle_2\right] \right\}, \tag{A 1b}$$

$$\mathcal{L}_2 \equiv \left\{ \left[\chi_b\left(\tfrac{\partial}{\partial t} - \tfrac{\partial}{\partial z}\right) - \tfrac{d\chi_b}{dz}\right], \left(\mathscr{C} - \tfrac{d\theta_b}{dz}\right)\left(\tfrac{\partial}{\partial t} - \tfrac{\partial}{\partial z} - \tfrac{d\theta_b}{dz}\right), \left(\tfrac{d\theta_b}{dz}\triangle_2\right) \right\}, \tag{A 1c}$$

$$\mathcal{L}_3 \equiv \left\{ 0, 0, \left[\left(\triangle + K_b^{-1}\tfrac{dK_b}{dz}\tfrac{\partial}{\partial z}\right)\triangle_2\right] \right\}, \tag{A 1d}$$

and

$$\hat{\boldsymbol{\mathcal{L}}} = (\hat{\mathcal{L}}_1, \hat{\mathcal{L}}_2, \hat{\mathcal{L}}_3)^{\mathrm{T}}\triangle_2, \tag{A 2a}$$

where $\hat{\mathcal{L}}_i$ $(i = 1, 2, 3)$ is the $i$-th row of the matrix $\hat{\boldsymbol{\mathcal{L}}}$ and given by

$$\hat{\mathcal{L}}_1 \equiv (0, 0, 0), \hat{\mathcal{L}}_2 \equiv (0, 0, 0), \hat{\mathcal{L}}_3 \equiv (K_b^{-1}, 0, 0), \tag{A 2b}$$

and

$$\boldsymbol{\mathcal{N}}(\boldsymbol{q}, \boldsymbol{q}) \equiv -\left\{ \left[(\boldsymbol{\Omega}P)\cdot\boldsymbol{\nabla}\theta\right], \left[(\boldsymbol{\Omega}P)\cdot\boldsymbol{\nabla}\theta + \chi\left(\tfrac{\partial}{\partial t} - \tfrac{\partial}{\partial z}\right)\theta + \theta\left(\tfrac{\partial}{\partial t} - \tfrac{\partial}{\partial z}\right)\chi\right] \right\}^{\mathrm{T}}. \tag{A 3}$$

The expression for the $3 \times 3$ differential operator $\mathbf{L}^{(\mathrm{a})}$ is given below

$$\mathbf{L}^{(\mathrm{a})} = (\mathrm{L}_1^{(\mathrm{a})}, \mathrm{L}_2^{(\mathrm{a})}, \mathrm{L}_3^{(\mathrm{a})})^{\mathrm{T}}, \tag{A 4a}$$

$$\mathrm{L}_1^{(\mathrm{a})} \equiv \left[\left(\mathrm{D}^2 - \mathrm{D} - \alpha^2\right), -\chi_b\mathrm{D}, -\alpha^2 R_0 K_b^{-1}\right], \tag{A 4b}$$

$$\mathrm{L}_2^{(\mathrm{a})} \equiv \left[\mathscr{S}\mathrm{D}, (\theta_b - \mathscr{C})\mathrm{D}, 0\right], \tag{A 4c}$$

$$\mathrm{L}_3^{(\mathrm{a})} \equiv \left\{ -\frac{\mathrm{d}\theta_b}{\mathrm{d}z}, -\frac{\mathrm{d}\theta_b}{\mathrm{d}z}, \left[\mathrm{D}^2 - K_b^{-1}\frac{\mathrm{d}K_b}{\mathrm{d}z}\mathrm{D} - K_b^{-2}\left(\frac{\mathrm{d}^2K_b}{\mathrm{d}z^2}K_b - \frac{\mathrm{d}K_b}{\mathrm{d}z}\frac{\mathrm{d}K_b}{\mathrm{d}z} - \alpha^2\right)\right]\right\} \tag{A 4d}$$

and the boundary conditions $\mathbf{B}^{(\mathrm{a})}$ mean

$$\tilde{\boldsymbol{q}}_0^{(\mathrm{a})} = 0 \text{ at } z = 0, \quad \tilde{\boldsymbol{q}}_0^{(\mathrm{a})} = 0 \text{ or } \tilde{\theta}^{(\mathrm{a})} = \tilde{\chi}^{(\mathrm{a})} = \left(\mathrm{D} - \frac{\mathrm{d}K_b}{\mathrm{d}z} K_b^{-1}\right) \tilde{P}_0^{(\mathrm{a})} = 0 \text{ at } z = \delta \quad (\mathrm{A}\,4e)$$

The vector function $\boldsymbol{\mathcal{N}}_{10}(\Phi_{kp}; z)$ is given by

$$\widetilde{\mathbf{N}}_{10}(\Phi_{lp}; z) = \widetilde{\mathbf{N}}_1(\tilde{\boldsymbol{q}}_0, \tilde{\boldsymbol{q}}_0), \quad (\mathrm{A}\,5)$$

$$\widetilde{\mathbf{N}}_1(\tilde{\boldsymbol{q}}_j, \tilde{\boldsymbol{q}}_k) = (1 - \tfrac{1}{2}\delta_{jk}) \left[\widehat{\mathbf{N}}_1(\tilde{\boldsymbol{q}}_j, \tilde{\boldsymbol{q}}_k) + \widehat{\mathbf{N}}_1(\tilde{\boldsymbol{q}}_k, \tilde{\boldsymbol{q}}_j)\right], \quad (\mathrm{A}\,6)$$

$$\widehat{\mathbf{N}}_1(\tilde{\boldsymbol{q}}_j, \tilde{\boldsymbol{q}}_k) = \begin{pmatrix} \alpha^2(\Phi_{lp}\tilde{\theta}_k \mathrm{D}\tilde{P}_j - \tilde{P}_j \mathrm{D}\tilde{\theta}_k) \\ -(\alpha^2 \Phi_{lp} \mathrm{D}\tilde{P}_j + \mathrm{D}\tilde{\chi}_j)\tilde{\theta}_k - \tilde{\chi}_j \mathrm{D}\tilde{\theta}_k + \alpha^2 \tilde{P}_j \mathrm{D}\tilde{\theta}_k \\ -\frac{1}{2} K_b^{-1} \left[\mathrm{D}\tilde{K}_j \mathrm{D}\tilde{P}_k + \tilde{K}_j(\mathrm{D}^2\tilde{P}_k - 2\alpha^2 \tilde{P}_k)\right] \end{pmatrix}, \quad (\mathrm{A}\,7)$$

The systems for the $z$-dependent coefficients $\tilde{\boldsymbol{q}}_{10}$ and $\tilde{\boldsymbol{q}}_{11}$ are given below

$$\left(\mathbf{L}_{10} - R_0 \widehat{\mathbf{L}}\right) \tilde{\boldsymbol{q}}_{10} = R_1 \widehat{\mathbf{L}} \tilde{\boldsymbol{q}}_0 \quad (\mathrm{A}\,8a)$$

$$\left(\mathbf{L}_{11} - R_0 \widehat{\mathbf{L}}\right) \tilde{\boldsymbol{q}}_{11} = \widetilde{\mathbf{N}}_{11}(\Phi_{kp}; z) \quad (\mathrm{A}\,8b)$$

where the matrices $\mathbf{L}_{10}$,$\mathbf{L}_{11}$ and $\widehat{\mathbf{L}}$ have the same form as $\boldsymbol{\mathcal{L}}$ and $\hat{\boldsymbol{\mathcal{L}}}$, provided $\triangle_2$ and $\triangle$ are replaced by $-\alpha^2$ and $(\mathrm{D}^2 - \alpha^2)$ for (a) $-a_{kp}^2$ and $(\mathrm{D}^2 - a_{kp}^2)$ for (b) and $\partial/\partial t$,$\partial/\partial z$,$R$ are replaced respectively by 0,D,$R_0$ in both. The vector $\widetilde{\mathbf{N}}_{11}$ is given by

$$\widetilde{\mathbf{N}}_{11} \equiv \begin{pmatrix} \alpha^2(\Phi_{lp}\tilde{\theta}_0 \mathrm{D}\tilde{P}_0 - \tilde{P}_0 \mathrm{D}\tilde{\theta}_0) \\ -(\alpha^2 \Phi_{lp} \mathrm{D}\tilde{P}_0 + \mathrm{D}\tilde{\chi}_0)\tilde{\theta}_0 - \tilde{\chi}_0 \mathrm{D}\tilde{\theta}_0 + \alpha^2 \tilde{P}_0 \mathrm{D}\tilde{\theta}_0 \\ -\frac{1}{2} K_b^{-1} \left[\mathrm{D}\tilde{K}_0 \mathrm{D}\tilde{P}_0 + \tilde{K}_0(\mathrm{D}^2\tilde{P}_0 - 2\alpha^2 \tilde{P}_0)\right] \end{pmatrix} \quad (\mathrm{A}\,9)$$

where the expression for $\tilde{K}_0$ can be found from (3.23$a$) for $K_0$ when $\chi_0$ is replaced by $\tilde{\chi}_0$.

## REFERENCES


Amberg, G. & Homsy, G. 1993 Nonlinear analysis of buoyant convection in binary solidification with application to channel formation. *Journal of Fluid Mechanics* **252**, 79–98.

Anderson, D. & Worster, M. G. 1995 Weakly nonlinear analysis of convection in mushy layers during the solidification fo binary alloys. *Journal of Fluid Mechanics* **302**, 307–331.

Ascher, U. M., Mattheij, R. M. & Russell, R. D. 1995 *Numerical Solution of Boundary Value Problems for Ordinary Differential Equations*, 2nd edn. Philadelphia: SIAM.

Batchelor, G. 1994 *An Introduction to Fluid Dynamics*, 16th edn. Cambridge University Press.

Busse, F. 1967 The stability of finite amplitude cellular convection and its relation to an extremum principle. *Journal of Fluid Mechanics* **30**, 625–649.

Busse, F. 1978 Non-linear properties of thermal convection. *Rep. Prog. Phys.* **41**, 1929–1967.

Chandrasekar, S. 1981 *Hydrodynamic and Hydromagnetic Stability*. New York: Dover.

Chen, F. & Chen, C. 1991 Experimental study of directional solidification of aqueous ammonium chloride solution. *Journal of Fluid Mechanics* **227**, 567–586.

Chen, F., Lu, J. W. & Yang, T. L. 1994 Convective instability in ammonium chloride solution directionally solidified from below. *Journal of Fluid Mechanics* **276**, 163–187.

Chung, C. & Chen, F. 2000 Onset of plume convection in mushy layers. *Journal of Fluid Mechanics* **408**, 53–82.

Copley, S., Giamei, A., Johnson, S. & Hornbecker, M. 1970 The origin of freckles in unidirectionally solidified castings. *Metallurgical Transactions* **1**, 2193–2204.

Emms, P. & Fowler, A. 1994 Compositional convection in the solidification of binary alloys. *Journal of Fluid Mechanics* **262**, 111–139.

Fowler, A. 1985 The formation of freckles in binary alloys. *Journal of Applied Mathematics* **35**, 159–174.

Hills, R., Loper, D. & Roberts, P. 1983 A thermodynamically consistent model of a mushy zone. *Quarterly Journal of Mechanics and Applied Mathematics* **36** (4), 505–539.

Hoyle, R. 1998 Universal instabilities of rolls, squares and hexagons. In *Time-Dependent Nonlinear Convection* (ed. P. Tyvand), pp. 51–82. Computational Mechanics Publications.

Iooss, G. & Joseph, D. 1990 *Elementary Stability and Bifurcation Theory*, 2nd edn. Springer.

Keller, H. B. 1976 *Numerical Solution of Two Point Boundary Value Problems*. SIAM.

Lage, J. 1998 The fundamental theory of flow through permeable media from darcy to turbulence. In *Transport Phenomena in Porous Media* (ed. D. Ingham & I. Pop), pp. 1–30. Oxford, UK: Pergamon.

Nield, D. 1998 Instability and turbulence in convective flows in porous media. In *Nonlinear Instability, Chaos and Turbulence* (ed. L. Debnath & D. Riahi), pp. 225–276. UK: WIT Press.

Roberts, P. & Loper, D. 1983 Towards a theory of the structure and evolution of a dendrite layer. In *Stellar and Planetary Magnetism* (ed. A. Soward), pp. 329–349. New York: Gordon and Breach.

Tait, S., Jahrling, K. & Jaupart, C. 1992 The planform of compositional convection and chimney formation in a mushy layer. *Nature* **359**, 406–408.

Worster, M. G. 1986 Solidification of an alloy from a cooled boundary. *Journal of Fluid Mechanics* **167**, 481–501.

Worster, M. G. 1991 Natural convection in a mushy layer. *Journal of Fluid Mechanics* **224**, 335–359.

Worster, M. G. 1992 Instabilities of the liquid and mushy regions during solidification of alloys. *Journal of Fluid Mechanics* **237**, 649–669.

**List of Recent TAM Reports**

| No. | Authors | Title | Date |
|---|---|---|---|
| 976 | Fried, E., and V. A. Korchagin | Striping of nematic elastomers—*International Journal of Solids and Structures* **39**, 3451–3467 (2002) | Aug. 2001 |
| 977 | Riahi, D. N. | On nonlinear convection in mushy layers: Part I. Oscillatory modes of convection—*Journal of Fluid Mechanics* **467**, 331–359 (2002) | Sept. 2001 |
| 978 | Sofronis, P., I. M. Robertson, Y. Liang, D. F. Teter, and N. Aravas | Recent advances in the study of hydrogen embrittlement at the University of Illinois—Invited paper, Hydrogen–Corrosion Deformation Interactions (Sept. 16–21, 2001, Jackson Lake Lodge, Wyo.) | Sept. 2001 |
| 979 | Fried, E., M. E. Gurtin, and K. Hutter | A void-based description of compaction and segregation in flowing granular materials—*Continuum Mechanics and Thermodynamics*, in press (2003) | Sept. 2001 |
| 980 | Adrian, R. J., S. Balachandar, and Z.-C. Liu | Spanwise growth of vortex structure in wall turbulence—*Korean Society of Mechanical Engineers International Journal* **15**, 1741–1749 (2001) | Sept. 2001 |
| 981 | Adrian, R. J. | Information and the study of turbulence and complex flow—*Japanese Society of Mechanical Engineers Journal B*, in press (2002) | Oct. 2001 |
| 982 | Adrian, R. J., and Z.-C. Liu | Observation of vortex packets in direct numerical simulation of fully turbulent channel flow—*Journal of Visualization*, in press (2002) | Oct. 2001 |
| 983 | Fried, E., and R. E. Todres | Disclinated states in nematic elastomers—*Journal of the Mechanics and Physics of Solids* **50**, 2691–2716 (2002) | Oct. 2001 |
| 984 | Stewart, D. S. | Towards the miniaturization of explosive technology—Proceedings of the 23rd International Conference on Shock Waves (2001) | Oct. 2001 |
| 985 | Kasimov, A. R., and Stewart, D. S. | Spinning instability of gaseous detonations—*Journal of Fluid Mechanics* (submitted) | Oct. 2001 |
| 986 | Brown, E. N., N. R. Sottos, and S. R. White | Fracture testing of a self-healing polymer composite—*Experimental Mechanics* (submitted) | Nov. 2001 |
| 987 | Phillips, W. R. C. | Langmuir circulations—*Surface Waves* (J. C. R. Hunt and S. Sajjadi, eds.), in press (2002) | Nov. 2001 |
| 988 | Gioia, G., and F. A. Bombardelli | Scaling and similarity in rough channel flows—*Physical Review Letters* **88**, 014501 (2002) | Nov. 2001 |
| 989 | Riahi, D. N. | On stationary and oscillatory modes of flow instabilities in a rotating porous layer during alloy solidification—*Journal of Porous Media* **6**, 1–11 (2003) | Nov. 2001 |
| 990 | Okhuysen, B. S., and D. N. Riahi | Effect of Coriolis force on instabilities of liquid and mushy regions during alloy solidification—*Physics of Fluids* (submitted) | Dec. 2001 |
| 991 | Christensen, K. T., and R. J. Adrian | Measurement of instantaneous Eulerian acceleration fields by particle-image accelerometry: Method and accuracy—*Experimental Fluids* (submitted) | Dec. 2001 |
| 992 | Liu, M., and K. J. Hsia | Interfacial cracks between piezoelectric and elastic materials under in-plane electric loading—*Journal of the Mechanics and Physics of Solids* **51**, 921–944 (2003) | Dec. 2001 |
| 993 | Panat, R. P., S. Zhang, and K. J. Hsia | Bond coat surface rumpling in thermal barrier coatings—*Acta Materialia* **51**, 239–249 (2003) | Jan. 2002 |
| 994 | Aref, H. | A transformation of the point vortex equations—*Physics of Fluids* **14**, 2395–2401 (2002) | Jan. 2002 |
| 995 | Saif, M. T. A, S. Zhang, A. Haque, and K. J. Hsia | Effect of native $Al_2O_3$ on the elastic response of nanoscale aluminum films—*Acta Materialia* **50**, 2779–2786 (2002) | Jan. 2002 |
| 996 | Fried, E., and M. E. Gurtin | A nonequilibrium theory of epitaxial growth that accounts for surface stress and surface diffusion—*Journal of the Mechanics and Physics of Solids* **51**, 487–517 (2003) | Jan. 2002 |
| 997 | Aref, H. | The development of chaotic advection—*Physics of Fluids* **14**, 1315–1325 (2002); see also *Virtual Journal of Nanoscale Science and Technology*, 11 March 2002 | Jan. 2002 |

**List of Recent TAM Reports (cont'd)**

| *No.* | *Authors* | *Title* | *Date* |
|---|---|---|---|
| 998 | Christensen, K. T., and R. J. Adrian | The velocity and acceleration signatures of small-scale vortices in turbulent channel flow—*Journal of Turbulence*, in press (2002) | Jan. 2002 |
| 999 | Riahi, D. N. | Flow instabilities in a horizontal dendrite layer rotating about an inclined axis—*Journal of Porous Media*, in press (2003) | Feb. 2002 |
| 1000 | Kessler, M. R., and S. R. White | Cure kinetics of ring-opening metathesis polymerization of dicyclopentadiene—*Journal of Polymer Science A* **40**, 2373–2383 (2002) | Feb. 2002 |
| 1001 | Dolbow, J. E., E. Fried, and A. Q. Shen | Point defects in nematic gels: The case for hedgehogs—*Archive for Rational Mechanics and Analysis*, in press (2004) | Feb. 2002 |
| 1002 | Riahi, D. N. | Nonlinear steady convection in rotating mushy layers—*Journal of Fluid Mechanics* **485**, 279–306 (2003) | Mar. 2002 |
| 1003 | Carlson, D. E., E. Fried, and S. Sellers | The totality of soft-states in a neo-classical nematic elastomer—*Journal of Elasticity* **69**, 169–180 (2003) with revised title | Mar. 2002 |
| 1004 | Fried, E., and R. E. Todres | Normal-stress differences and the detection of disclinations in nematic elastomers—*Journal of Polymer Science B: Polymer Physics* **40**, 2098–2106 (2002) | June 2002 |
| 1005 | Fried, E., and B. C. Roy | Gravity-induced segregation of cohesionless granular mixtures—*Lecture Notes in Mechanics*, in press (2002) | July 2002 |
| 1006 | Tomkins, C. D., and R. J. Adrian | Spanwise structure and scale growth in turbulent boundary layers—*Journal of Fluid Mechanics* (submitted) | Aug. 2002 |
| 1007 | Riahi, D. N. | On nonlinear convection in mushy layers: Part 2. Mixed oscillatory and stationary modes of convection—*Journal of Fluid Mechanics* **517**, 71–102 (2004) | Sept. 2002 |
| 1008 | Aref, H., P. K. Newton, M. A. Stremler, T. Tokieda, and D. L. Vainchtein | Vortex crystals—*Advances in Applied Mathematics* **39**, in press (2002) | Oct. 2002 |
| 1009 | Bagchi, P., and S. Balachandar | Effect of turbulence on the drag and lift of a particle—*Physics of Fluids*, in press (2003) | Oct. 2002 |
| 1010 | Zhang, S., R. Panat, and K. J. Hsia | Influence of surface morphology on the adhesive strength of aluminum/epoxy interfaces—*Journal of Adhesion Science and Technology* **17**, 1685–1711 (2003) | Oct. 2002 |
| 1011 | Carlson, D. E., E. Fried, and D. A. Tortorelli | On internal constraints in continuum mechanics—*Journal of Elasticity* **70**, 101–109 (2003) | Oct. 2002 |
| 1012 | Boyland, P. L., M. A. Stremler, and H. Aref | Topological fluid mechanics of point vortex motions—*Physica D* **175**, 69–95 (2002) | Oct. 2002 |
| 1013 | Bhattacharjee, P., and D. N. Riahi | Computational studies of the effect of rotation on convection during protein crystallization—*International Journal of Mathematical Sciences*, in press (2004) | Feb. 2003 |
| 1014 | Brown, E. N., M. R. Kessler, N. R. Sottos, and S. R. White | *In situ* poly(urea-formaldehyde) microencapsulation of dicyclopentadiene—*Journal of Microencapsulation* (submitted) | Feb. 2003 |
| 1015 | Brown, E. N., S. R. White, and N. R. Sottos | Microcapsule induced toughening in a self-healing polymer composite—*Journal of Materials Science* (submitted) | Feb. 2003 |
| 1016 | Kuznetsov, I. R., and D. S. Stewart | Burning rate of energetic materials with thermal expansion—*Combustion and Flame* (submitted) | Mar. 2003 |
| 1017 | Dolbow, J., E. Fried, and H. Ji | Chemically induced swelling of hydrogels—*Journal of the Mechanics and Physics of Solids*, in press (2003) | Mar. 2003 |
| 1018 | Costello, G. A. | Mechanics of wire rope—Mordica Lecture, Interwire 2003, Wire Association International, Atlanta, Georgia, May 12, 2003 | Mar. 2003 |
| 1019 | Wang, J., N. R. Sottos, and R. L. Weaver | Thin film adhesion measurement by laser induced stress waves—*Journal of the Mechanics and Physics of Solids* (submitted) | Apr. 2003 |

**List of Recent TAM Reports (cont'd)**

| *No.* | *Authors* | *Title* | *Date* |
|---|---|---|---|
| 1020 | Bhattacharjee, P., and D. N. Riahi | Effect of rotation on surface tension driven flow during protein crystallization—*Microgravity Science and Technology* **14**, 36–44 (2003) | Apr. 2003 |
| 1021 | Fried, E. | The configurational and standard force balances are not always statements of a single law—*Proceedings of the Royal Society* (submitted) | Apr. 2003 |
| 1022 | Panat, R. P., and K. J. Hsia | Experimental investigation of the bond coat rumpling instability under isothermal and cyclic thermal histories in thermal barrier systems—*Proceedings of the Royal Society of London A* **460**, 1957–1979 (2003) | May 2003 |
| 1023 | Fried, E., and M. E. Gurtin | A unified treatment of evolving interfaces accounting for small deformations and atomic transport: grain-boundaries, phase transitions, epitaxy—*Advances in Applied Mechanics* **40**, 1–177 (2004) | May 2003 |
| 1024 | Dong, F., D. N. Riahi, and A. T. Hsui | On similarity waves in compacting media—*Horizons in World Physics* **244**, 45–82 (2004) | May 2003 |
| 1025 | Liu, M., and K. J. Hsia | Locking of electric field induced non-180° domain switching and phase transition in ferroelectric materials upon cyclic electric fatigue—*Applied Physics Letters* **83**, 3978–3980 (2003) | May 2003 |
| 1026 | Liu, M., K. J. Hsia, and M. Sardela Jr. | In situ X-ray diffraction study of electric field induced domain switching and phase transition in PZT-5H—*Journal of the American Ceramics Society* (submitted) | May 2003 |
| 1027 | Riahi, D. N. | On flow of binary alloys during crystal growth—*Recent Research Development in Crystal Growth*, in press (2003) | May 2003 |
| 1028 | Riahi, D. N. | On fluid dynamics during crystallization—*Recent Research Development in Fluid Dynamics*, in press (2003) | July 2003 |
| 1029 | Fried, E., V. Korchagin, and R. E. Todres | Biaxial disclinated states in nematic elastomers—*Journal of Chemical Physics* **119**, 13170–13179 (2003) | July 2003 |
| 1030 | Sharp, K. V., and R. J. Adrian | Transition from laminar to turbulent flow in liquid filled microtubes—*Physics of Fluids* (submitted) | July 2003 |
| 1031 | Yoon, H. S., D. F. Hill, S. Balachandar, R. J. Adrian, and M. Y. Ha | Reynolds number scaling of flow in a Rushton turbine stirred tank: Part I—Mean flow, circular jet and tip vortex scaling—*Chemical Engineering Science* (submitted) | Aug. 2003 |
| 1032 | Raju, R., S. Balachandar, D. F. Hill, and R. J. Adrian | Reynolds number scaling of flow in a Rushton turbine stirred tank: Part II—Eigen-decomposition of fluctuation—*Chemical Engineering Science* (submitted) | Aug. 2003 |
| 1033 | Hill, K. M., G. Gioia, and V. V. Tota | Structure and kinematics in dense free-surface granular flow—*Physical Review Letters*, in press (2003) | Aug. 2003 |
| 1034 | Fried, E., and S. Sellers | Free-energy density functions for nematic elastomers—*Journal of the Mechanics and Physics of Solids* **52**, 1671–1689 (2004) | Sept. 2003 |
| 1035 | Kasimov, A. R., and D. S. Stewart | On the dynamics of self-sustained one-dimensional detonations: A numerical study in the shock-attached frame—*Physics of Fluids* (submitted) | Nov. 2003 |
| 1036 | Fried, E., and B. C. Roy | Disclinations in a homogeneously deformed nematic elastomer—*Nature Materials* (submitted) | Nov. 2003 |
| 1037 | Fried, E., and M. E. Gurtin | The unifying nature of the configurational force balance—*Mechanics of Material Forces* (P. Steinmann and G. A. Maugin, eds.), in press (2003) | Dec. 2003 |
| 1038 | Panat, R., K. J. Hsia, and J. W. Oldham | Rumpling instability in thermal barrier systems under isothermal conditions in vacuum—*Philosophical Magazine*, in press (2004) | Dec. 2003 |
| 1039 | Cermelli, P., E. Fried, and M. E. Gurtin | Sharp-interface nematic–isotropic phase transitions without flow—*Archive for Rational Mechanics and Analysis* **174**, 151–178 (2004) | Dec. 2003 |
| 1040 | Yoo, S., and D. S. Stewart | A hybrid level-set method in two and three dimensions for modeling detonation and combustion problems in complex geometries—*Combustion Theory and Modeling* (submitted) | Feb. 2004 |

**List of Recent TAM Reports (cont'd)**

| *No.* | *Authors* | *Title* | *Date* |
|---|---|---|---|
| 1041 | Dienberg, C. E., S. E. Ott-Monsivais, J. L. Ranchero, A. A. Rzeszutko, and C. L. Winter | Proceedings of the Fifth Annual Research Conference in Mechanics (April 2003), TAM Department, UIUC (E. N. Brown, ed.) | Feb. 2004 |
| 1042 | Kasimov, A. R., and D. S. Stewart | Asymptotic theory of ignition and failure of self-sustained detonations—*Journal of Fluid Mechanics* (submitted) | Feb. 2004 |
| 1043 | Kasimov, A. R., and D. S. Stewart | Theory of direct initiation of gaseous detonations and comparison with experiment—*Proceedings of the Combustion Institute* (submitted) | Mar. 2004 |
| 1044 | Panat, R., K. J. Hsia, and D. G. Cahill | Evolution of surface waviness in thin films via volume and surface diffusion—*Journal of Applied Physics* (submitted) | Mar. 2004 |
| 1045 | Riahi, D. N. | Steady and oscillatory flow in a mushy layer—*Current Topics in Crystal Growth Research*, in press (2004) | Mar. 2004 |
| 1046 | Riahi, D. N. | Modeling flows in protein crystal growth—*Current Topics in Crystal Growth Research*, in press (2004) | Mar. 2004 |
| 1047 | Bagchi, P., and S. Balachandar | Response of the wake of an isolated particle to isotropic turbulent cross-flow—*Journal of Fluid Mechanics* (submitted) | Mar. 2004 |
| 1048 | Brown, E. N., S. R. White, and N. R. Sottos | Fatigue crack propagation in microcapsule toughened epoxy—*Journal of Materials Science* (submitted) | Apr. 2004 |
| 1049 | Zeng, L., S. Balachandar, and P. Fischer | Wall-induced forces on a rigid sphere at finite Reynolds number—*Journal of Fluid Mechanics* (submitted) | May 2004 |
| 1050 | Dolbow, J., E. Fried, and H. Ji | A numerical strategy for investigating the kinetic response of stimulus-responsive hydrogels—*Journal of the Mechanics and Physics of Solids* (submitted) | June 2004 |
| 1051 | Riahi, D. N. | Effect of permeability on steady flow in a dendrite layer—*Journal of Porous Media*, in press (2004) | July 2004 |
| 1052 | Cermelli, P., E. Fried, and M. E. Gurtin | Transport relations for surface integrals arising in the formulation of balance laws for evolving fluid interfaces—*Journal of Fluid Mechanics* (submitted) | Sept. 2004 |
| 1053 | Stewart, D. S., and A. R. Kasimov | Theory of detonation with an embedded sonic locus—*SIAM Journal on Applied Mathematics* (submitted) | Oct. 2004 |
| 1054 | Stewart, D. S., K. C. Tang, S. Yoo, M. Q. Brewster, and I. R. Kuznetsov | Multi-scale modeling of solid rocket motors: Time integration methods from computational aerodynamics applied to stable quasi-steady motor burning—*Proceedings of the 43rd AIAA Aerospace Sciences Meeting and Exhibit* (January 2005), Paper AIAA-2005-0357 (2005) | Oct. 2004 |
| 1055 | Ji, H., H. Mourad, E. Fried, and J. Dolbow | Kinetics of thermally induced swelling of hydrogels—*International Journal of Solids and Structures* (submitted) | Dec. 2004 |
| 1056 | Fulton, J. M., S. Hussain, J. H. Lai, M. E. Ly, S. A. McGough, G. M. Miller, R. Oats, L. A. Shipton, P. K. Shreeman, D. S. Widrevitz, and E. A. Zimmermann | Final reports: Mechanics of complex materials, Summer 2004 (K. M. Hill and J. W. Phillips, eds.) | Dec. 2004 |
| 1057 | Hill, K. M., G. Gioia, and D. R. Amaravadi | Radial segregation patterns in rotating granular mixtures: Waviness selection—*Physical Review Letters*, in press (2004) | Dec. 2004 |
| 1058 | Riahi, D. N. | Nonlinear oscillatory convection in rotating mushy layers—*Journal of Fluid Mechanics* (submitted) | Dec. 2004 |
| 1059 | Okhuysen, B. S., and D. N. Riahi | On buoyant convection in binary solidification—*Journal of Fluid Mechanics* (submitted) | Jan. 2005 |